TITLE: **DYNAMIC LATERAL EARTH PRESSURE ON UNDERGROUND STRUCTURES**

GRANT: F49620-98-1-0109

Authors: Sam M.B. Helwany, Assistant Professor
Department of Civil Engineering and Mechanics
University of Wisconsin-Milwaukee
P.O. Box 784
Milwaukee, WI 53201
Phone: 414-229-4131
Fax: 414-229-6958
Email: helwany@uwm.edu

Asadul Chowdhury, Manager-Repository Design, Construction, Operation
Center of Nuclear Waste Regulatory Analyses
Southwest Research Institute
6220 Culebra Rd.
San Antonio, TX 78238
Phone: 210-522-5151
Fax: 210-522-6081
Email: achowdhury@swri.edu

Keywords: Soil-Structure Interaction, Impulse Loading, Wave Propagation, Underground Structures, Large-scale Laboratory Impulse Tests, Three-dimensional Finite Element Analysis.

REPORT DOCUMENTATION PAGE

98

AFRL-SR-BL-TR-00-

0515

1. AGENCY USE ONLY *(Leave blank)*	2. REPORT DATE	3. REPORT TYPE AND DATES COVERED
	20 September 2000	FINAL: 15 Nov 97 To 14 Nov 99

4. TITLE AND SUBTITLE
DYNAMIC LATERAL EARTH PRESSURE ON UNDERGROUND STRUCTURES

5. FUNDING NUMBERS
F49620-98-1-0109

6. AUTHOR(S)
Sam M.B. Helwany, Assistant Professor
Asadul Chowdhury, Manager-Repository Design, Construction, Operation

7. PERFORMING ORGANIZATION NAME(S) AND ADDRESS(ES)
University of Wisconsin-Milwaukee
P.O. Box 784
Milwaukee, WI 53201

8. PERFORMING ORGANIZATION REPORT NUMBER

9. SPONSORING/MONITORING AGENCY NAME(S) AND ADDRESS(ES)
AIR FORCE OFFICE OF SCIENTIFIC RESEARCH
801 North Randolph St.
Arlington VA 22203-1977

10. SPONSORING/MONITORING AGENCY REPORT NUMBER

11. SUPPLEMENTARY NOTES

12a. DISTRIBUTION AVAILABILITY STATEMENT
Approved for public release; distribution unlimited

12b. DISTRIBUTION CODE

13. ABSTRACT *(Maximum 200 words)*

The dynamic lateral earth pressures resulting from underground detonation can cause severe damage to underground structures. The shock exerted on an underground structure caused by an underground explosion will vary with the detonation depth, the intensity of detonation force, and distance of detonation source from the underground structure. This stud3' includes a preliminary investigation of the lateral propagation and attenuation of shock waves, and the · accompanying response of a subsection of an underground structure, caused by an underground shock (impulse load) emanating from a source located within the soil adjacent to the structure. This paper describes four large-scale impulse tests on a 1.0 m-high prototype subsection of an underground structure subjected to controlled impulsive lateral loadings propagating through a 0.75 m-thick backfill soil. The response of the subsection to the impulsive loading is carefully monitored utilizing an extensive instrumentation program. The test results provide insight into the phenomenon of shock wave propagation caused by an impulsive loading emanating from an underground source adjacent to the underground structure. The tests indicated that the damaging effect of impulse loading increased with surcharge pressure (depth) until a "threshold" surcharge pressure is reached above which the damaging effect of impulse loading decreased.

14. SUBJECT TERMS
INTERACTION BETWEEN SOIL AND UNDERGROUND STRUCTURES DURING LATERAL IMPULSE LOADING

15. NUMBER OF PAGES

16. PRICE CODE

17. SECURITY CLASSIFICATION OF REPORT	18. SECURITY CLASSIFICATION OF THIS PAGE	19. SECURITY CLASSIFICATION OF ABSTRACT	20. LIMITATION OF ABSTRACT

ABSTRACT

The dynamic lateral earth pressures resulting from underground detonation can cause severe damage to underground structures. The shock exerted on an underground structure caused by an underground explosion will vary with the detonation depth, the intensity of detonation force, and distance of detonation source from the underground structure. This study includes a preliminary investigation of the lateral propagation and attenuation of shock waves, and the accompanying response of a subsection of an underground structure, caused by an underground shock (impulse load) emanating from a source located within the soil adjacent to the structure. This paper describes four large-scale impulse tests on a 1.0 m-high prototype subsection of an underground structure subjected to controlled impulsive lateral loadings propagating through a 0.75 m-thick backfill soil. The response of the subsection to the impulsive loading is carefully monitored utilizing an extensive instrumentation program. The test results provide insight into the phenomenon of shock wave propagation caused by an impulsive loading emanating from an underground source adjacent to the underground structure. The tests indicated that the damaging effect of impulse loading increased with surcharge pressure (depth) until a "threshold" surcharge pressure is reached above which the damaging effect of impulse loading decreased.

INTERACTION BETWEEN SOIL AND UNDERGROUND STRUCTURES DURING LATERAL IMPULSE LOADING

INTRODUCTION

Underground structures such as civil defense facilities may be damaged by impulsive lateral earth pressures resulting from adjacent underground detonation. The dynamic forces exerted on an underground structure, buried 10-20 meters deep in soil, as caused by an underground detonation, will vary with detonation depth, rise time of detonation force, and distance of detonation from the underground structure. Determination of the effects of detonation depth, rise time of detonation force, and distance of detonation in different soil types and various drainage conditions is essential for the safety of important underground structures. This paper describes a preliminary experimental investigation of the lateral propagation and attenuation of shock waves, and the accompanying response of a model subsection of an underground structure, caused by an underground shock emanating from a source located within the soil adjacent to the structure.

In this study, a 1.0 m-high prototype subsection (i.e., similitude rules are not utilized) of a typical underground structure, shown in Figures 1 and 2, is subjected to controlled impulsive loadings propagating through the 0.75 m-thick backfill soil. This laboratory test is termed "impulse test". Four impulse tests are conducted utilizing a dry sand backfill material subjected to different surcharge pressures and impulse loads. The response of the subsection is carefully measured utilizing an extensive instrumentation program. The test results provide insight into the phenomenon of shock wave propagation caused by an impulsive loading emanating from a source adjacent to the underground structure, with special emphasis on the effects of surcharge pressure (function of depth) and impulse intensity.

BACKGROUND

Natural earthquakes and conventional or nuclear underground explosions are two major sources of dynamic loading on underground structures. A general description of the ground motion which occurs due to dynamic loading is given by Gere and Shah (1984). A comparison of ground motions produced by an earthquake and underground explosions is provided by Vortman (1981). Due to the different mechanisms of wave generation in earthquakes and underground explosions, and wave attenuation and dispersion during transmission, the underground structures respond in different ways to the ground motions caused by these two different types of dynamic loading.

An underground explosion releases a large quantity of energy including generation of gaseous products, in a very short length of time (milliseconds). After energy release occurs, dynamic waves of several types such as P-waves and S-waves are generated, and their characteristics change with distance of propagation, the type of material through which they travel, and interaction with the underground structure, the surface, and other boundaries. Compared to the duration of earthquake waves, shock waves caused by underground explosions are rather short duration pulses so long as they are felt in a direct line relatively near the source (Vortman, 1979). However, when reflections from the surface and other boundaries take place before they are felt at a target structure, they tend to be smeared out to a longer duration. Thus, amplitudes, frequency content, and durations are all subject to the location and distance of the sensing point from the source of energy release, as in the case for earthquakes. Further, the time histories tend to change from a relatively short to a somewhat longer duration transient random excitation,

although the duration is usually much less than that of earthquakes.

The soil-structure interaction problems for underground protective structures under explosive threats have received considerable attention in the last few decades. Work prior to 1963 is described in the Proceedings of the Symposium on Soil-Structure Interaction published by the University of Arizona in 1967 and more recent developments have been described by Gill (1967), Palacios and Kennedy (1967), Balsara and Cummins (1968), Albritton (1968), Allgood (1970), Ghaboussi et al. (1984), Slawson (1984), Getchell et al. (1984), Puglisi and Krauthammer (1987), Weidlinger and Hinman (1988), Chen et al. (1990), and Chen and Chen (1996). It is noteworthy, however, that most of these studies are limited to investigations of shallow-buried structures subjected to static and/or dynamic overpressures caused by air-blast.

LARGE-SCALE IMPULSE TESTS

Four large-scale laboratory impulse tests on an instrumented 12.7 mm-thick aluminum target plate, measuring 107 cm-high and 110 cm-wide, are conducted in a newly-devised impulse test apparatus shown in Figure 2. The instrumented target plate represents a subsection of the full size underground structure as indicated in Figure 1. The impulsive stresses are applied to the soil specimen utilizing a 30 cm-diameter rigid loading plate and an impulse generator. The main objective of these tests is to investigate the lateral propagation and attenuation of shock waves, and the accompanying response of a model subsection of an underground structure, caused by an underground shock emanating from a source located within the soil adjacent to the structure. The impulse test results provide insight into the phenomenon of shock wave propagation caused by impulsive loadings. Test results can also be very useful for validation of physical and numerical

modeling techniques, such as centrifugal modeling and finite element modeling, by comparing their results with the results of the impulse tests.

During ground shaking resulting from an underground explosion, a soil subsection in the ground is subjected to a complex system of deformations resulting from the erratic sequence of ground motions. In this case, the major soil deformations may be attributed to the propagation of ground shock from the source of detonation. A soil subsection, such as that shown in Figure 1, may be considered to be subjected to an impulsive loading that is applied for a very short period of time.

The impulse test apparatus, shown in Figure 2, is a rigid soil box measuring approximately 1.14 m high, 1.11 m wide, and 0.90 m deep (inside dimensions). The test apparatus is rigidly mounted on a strong floor and a strong wall as indicated in the same figure. The 12.7 mm-thick aluminum target plate, which represents a 1.07 m x 1.1 m subsection of an underground structure, is made slightly smaller than the soil box and connected to the strong wall at each corner utilizing four load cells as shown in the same figure.

As indicated in Figure 2, the thickness of the soil specimen of 0.75 m is purposely made smaller than the width and height of the apparatus to reduce the boundary effects on the propagation of the compression wave (primary stress wave) in the horizontal direction. The compression wave emanating from the loading plate will travel horizontally a relatively short distance (0.75 m) before arriving at the target plate. Because of the finite dimensions of the test apparatus, however, the reflected waves from the boundaries of the test apparatus will arrive at the target plate soon after the first arrival of the compression wave. Of great interest is the peak response of the target plate which corresponds to the "first arrival" of the compression wave at

the target plate. Stress waves arriving at the target plate with delay (i.e., after the first arrival) are mainly due to the imposed boundary conditions and may contaminate the measured response.

In light of the above, it can be presumed that the field "loading" conditions shown in Figure 1 are correctly simulated in the impulse test apparatus, even though the "free field" condition is not met. Again, the main interest is to obtain the peak response of the target plate which is most likely to be associated with the first arrival of the compression wave. Also, one of the objectives of performing the impulse tests is to utilize their measured results to validate future centrifugal and numerical modeling. Therefore, the impulse test can be considered as a "prototype boundary value problem" which is to be modeled numerically and in the centrifuge for verification purposes. The numerical and centrifugal models are capable of simulating the "artificial" boundary conditions of the prototype.

For accurate simulation of field conditions the following factors are considered in the design of the impulse test apparatus:

1. To ensure uniformity of the sand backfill, the soil is prepared by pluvial deposition using a raining device. This raining device is simply a "sand spreader" that consists of a sand hopper and a sieve which can move horizontally at a pre-specified constant speed. The sand spreader can also move vertically in order to keep the "height of drop" constant. The flow from the hopper is controlled by an adjustable slot which governs the intensity of the sand rain, and thus the density of the deposited layer (as established by Kolbuszewski, 1948). The raining device was calibrated to consistently produce a uniform density of approximately 16.3 kN/m^3 for the silica sand yielding an estimated in-situ relative density

of approximately 70 percent. The maximum and minimum unit weights of the sand are 17.1 kN/m^3 and 14.9 kN/m^3, respectively. The particle size distribution curve of the sand is shown in Figure 3. The effective particle size, $D_{10}=0.33$ mm, coefficient of uniformity, $D_{60}/D_{10}=C_u=1.8$, and coefficient of curvature, $C_c=(D_{30})^2/(D_{60} \times D_{10})=1.05$.

2. Uniform normal stress (surcharge) is applied on top of the backfill in the impulse test utilizing an air bag. The air pressure in the air bag simulates the depth at which the modeled soil subsection is selected.

3. The impulse tests are instrumented as shown in Figures 2 and 4. A number of different instruments are used, as indicated in Table 1, including 10 piezoelectric accelerometers and 11 piezoelectric strain gages (Figure 4). All measurements are recorded automatically using a high speed data acquisition system. This data acquisition system is capable of acquiring 40 channels of data at frequencies up to 1 MHz per channel. The capability of acquiring data at such a high frequency is essential for the impulse tests in which the impulsive loads are applied in a very short length of time (10-20 milliseconds). The instrumentation program also included seven interface pressure sensors and four load cells (Table 1) which are supposedly capable of measuring the interactive lateral earth pressure between the soil and the target plate, and the total force exerted on the target plate, respectively. Unfortunately, these sensors yielded erroneous measurements caused by bending of the target plate during dynamic load application. Nevertheless, advanced numerical modeling, such as three-dimensional finite element analysis with the correct

constitutive modeling of the materials involved and the correct interface modeling, can be employed to back-calculate the dynamic lateral earth pressure exerted on the target plate. An example of such analysis to calculate the dynamic lateral earth pressure on the target plate is described in a later section.

4. The impulsive stresses are applied to the soil specimen in the impulse test utilizing a hydraulic actuator (impulse generator) which is capable of applying impulsive loads up to 45 kN within 5 ms at an estimated velocity of 254 cm/sec (low velocity impact). The impulse generator is equipped with a robust load cell and an LVDT allowing direct and complete measurements of the applied impulse load. Impulse load histories for tests 1, 2, 3, and 4 are shown in Figure 5.

TEST RESULTS

The loading conditions associated with the impulse tests, which are conducted under otherwise similar conditions, are listed in Table 2. To achieve appropriate impulse intensities, the impulse generator was programmed to travel a horizontal distance of 5 cm, at maximum hydraulic pressure, before striking the loading plate. In tests 1, 2, and 3, the impulse generator was programmed to travel an additional distance of approximately 6 mm after striking the loading plate (penetration distance). The resulting impulse load history, as measured by the load cell attached to the impulse generator, is shown in Figures 5(a), 5(b), and 5(c), corresponding to tests 1, 2, and 3, respectively. The penetration distance was doubled (approximately 12 mm) in test 4 resulting in the impulse load history shown in Figure 5(d). The measured peak impulse accelerations at the

center of the loading plate for all tests are listed in Table 2.

A direct comparison between the measured results of tests 1, 2, and 3, which are conducted at surcharge pressures of 35 kPa, 70 kPa, and 105 kPa, respectively, will illustrate the effects of surcharge pressure on the response of the target plate due to essentially similar impulse load histories utilized in these tests. Also, a direct comparison between the measured results of tests 2 and 4, which are conducted at an identical surcharge pressure of 70 kPa but subjected to different impulse load intensities, will illustrate the effects of impulse load intensity.

Instead of listing all the measured results for tests 1, 2, 3, and 4, only some of the measured results of test 4 will be presented herein as an example. Appendix A includes detailed measurements obtained for test 4. Figures 6 and 7 show detailed time histories of measured accelerations and strains at the center of the loading plate and the center of the target plate, respectively, for test 4. In these figures, t=0 is the time at which the data acquisition system started to collect data shortly before the impulse generator impacted the loading plate. The acceleration data plotted in Figure 6(a) indicate that the compression wave arrived at the inner side of the loading plate (in contact with backfill soil) at t=0.0103 s. The acceleration data plotted in Figure 6(b) indicate that the same compression wave reached the center of the target plate at t=0.0136 s. This means that the time required for the compression wave to travel through the 75 cm-thick sand layer is approximately 0.0033 s. Therefore, the estimated compression wave velocity of the sand is approximately 229 m/s. Utilizing Equation 1, an initial shear modulus for the sand of 29,075 kPa is calculated, assuming that the sand has a Poisson's ratio of 0.25, and a unit weight of 16.3 kN/m^3. Table 3 lists the measured p-wave velocities in the sand along with the calculated initial shear moduli (from Equation 1) for tests 1, 2, 3, and 4.

$$v_p=[\frac{2G(1-\nu)}{\rho(1-2\nu)}]^{\frac{1}{2}} \qquad \textit{Equation } 1$$

where,

v_p =p-wave velocity

G =shear modulus

ν =Poisson's ratio

ρ =soil density

As indicated earlier, the thickness of the soil specimen in the impulse test apparatus was purposely made smaller than the width and height of the test apparatus to reduce the boundary effects on the propagation of the compression wave in the horizontal direction. The compression wave emanating from the loading plate will travel horizontally a relatively short distance (0.75 m) before arriving at the target plate. Reflected waves from the boundaries of the test apparatus will arrive at the target plate soon after the first arrival of the compression wave and may contaminate the measured results.

Of great interest is the "peak" response of the target plate which corresponds to the "first arrival" of the compression wave at the target plate. The value of the peak response might be slightly affected by the boundaries of the test apparatus and by the arrival of the shear wave and other waves. In test 4, for example, the time required for the compression wave to travel from the loading plate to the target plate is approximately 3.3 ms (v_p = 229 m/s and Distance = 0.75 m). Considering point A in Figure 5(d) to be the peak of the impulse load occurring at t=22.2 ms, the peak of the compression wave is then expected to arrive at the target plate at

approximately 25.5 ms (= 22.2 ms+3.3 ms). Figure 7(b) shows that the peak response of the target plate (point P in the figure), in terms of strains, occurred soon after the estimated first arrival of the compression wave. This slight delay is caused be the flexibility of the target plate which deformed outward, following the first arrival of the compression wave, and reached its peak response at point P. Following the peak response, the target plate slightly oscillated several times while the measured dynamic response declined in a manner resembling the behavior of an over-damped system, as shown in Figure 7(b). The measured strain approached -2 $\mu\epsilon$ at approximately 2 seconds as indicated in the same figure.

The measured peak accelerations and peak strains corresponding to the first arrival of the compression wave at the target plate for test 4 are summarized in Figure 8. It is noted from Figure 8(a) that peak accelerations are relatively small with the maximum acceleration being located between the center and top of the target plate.

Measured peak strains, however, vary considerably in each test with the maximum tensile strain being at the center of the target plate, as shown in Figure 8(b). Also, small negative (compressive) strains were measured near the middle of the edges of the target plate. It is to be noted that all strain gages were installed on the outer face of the target plate (not in contact with soil) along a horizontal line and a vertical line passing though the center of the target plate. The strain gages installed along the horizontal line can only measure "horizontal" strains, whereas the strain gages along the vertical line can only measure "vertical" strains. Thus, at the center of the target plate both horizontal and vertical strains are measured. The measured horizontal and vertical strains at the center of the target plate in test 4 were asymmetric as indicated in Figure 8(b).

Effects of Overburden Pressure

A comparison between the measured peak accelerations on target plate for tests 1, 2, and 3 is shown in Figure 9(a). As indicated earlier, the soil specimens in tests 1, 2, and 3 were subjected to surcharge pressures of 35 kPa, 70 kPa, and 105 kPa, respectively. The applied impulse loadings in these three tests were essentially similar as indicated in Figures 5(a), 5(b), and 5(c), with impulse durations ranging from 15 to 20 ms, and peak normal stresses ranging from 220 kPa to 270 kPa. Figure 9(a) shows that the measured accelerations in test 1 were relatively small, and the measured accelerations in tests 2 and 3 were comparable and greater than those measured in test 1.

Similarly, Figure 9(b) indicates that the measured peak strains in the target plate were the smallest in test 1 (only vertical strains are compared in the figure). However, the measured peak strains in test 3, which was subjected to 105 kPa surcharge pressure, were substantially smaller (up to 40 percent) than those of test 2, which was subjected to 70 kPa surcharge pressure. This observation implies that the effect of impulse loading on the target plate is function of the surcharge pressure. The damaging effect of impulse loading increases with surcharge pressure (depth) until a threshold surcharge pressure is reached (70 kPa in this case). Above this threshold pressure, the damaging effect of impulse loading decreases. This can be attributed to the increase in soil strength as the confining pressure increases. This increase of soil strength with increasing surcharge pressure was indicated earlier in Table 3, where it was shown that the initial shear modulus of the soil, calculated from the measured p-wave velocity, increased with surcharge pressure. Undoubtedly, the above observation is based only on a limited number of tests, and further impulse tests with greater impulse intensities, and with a variety of soil environments and

conditions, are needed to ascertain such a conclusion.

Effects of Impulse Intensity

Test 2 and 4 were conducted under the same surcharge pressure of 70 kPa. The impulse loading applied in tests 2 and 4 are shown in Figures 5(b) and 5(d), respectively. The figures indicate that the impulse applied in test 4 is of greater magnitude and duration than that applied in test 2. Comparisons between peak accelerations and peak strains for tests 2 and 4 are shown in Figures 10(a) and 10(b), respectively. In the figures, a very substantial increase in acceleration and strain measurements on the target plate is noted in test 4 above those measured in test 2. This is mainly attributed to the greater impulse intensity applied in test 4.

Peak Dynamic Lateral Earth Pressure on Target Plate

The finite element method can be utilized to analyze the impulse tests to (1) gain insight into the complicated interaction between soil and the target plate under different confining pressures and different impulse loading, and (2) complement the testing program described in this paper by evaluating some of the responses which were not measured in the tests (e.g., the dynamic lateral earth pressure on target plate). As an example, three-dimensional finite element analysis of impulse test 4 is briefly described herein with the objective of calculating the peak dynamic lateral earth pressure exerted on the target plate. As indicated earlier, the interface pressure censors utilized in the impulse tests yielded erroneous results because of target plate bending during loading, thus, the finite element is utilized herein to predict the peak dynamic lateral earth pressure exerted on the target plate as a substitute for measurements.

The finite element computer program DYNA3D (Hallquist 1982), developed at Lawrence Livermore National Laboratory, is utilized for the analysis. This finite element code is well-suited for analyzing the dynamic response of three-dimensional solids and structures. It is based on a finite element discretization of the three spatial dimensions and a finite difference discretization of time. The explicit central difference method is used to integrate the equations of motion in time. The element formulations available include one-dimensional truss and beam elements, two-dimensional quadrilateral and triangular shell elements, and three-dimensional continuum elements. Many material models are available to represent a wide range of material behavior, including elasticity, plasticity, thermal effects, and rate dependence. In addition, DYNA3D has a sophisticated contact interface capability, including frictional sliding, separation, and single surface contact, to handle a range of mechanical interactions between independent bodies. This capability is essential for the analyses of the impulse tests.

The finite element discretization of the impulse test is shown in Figure 11. The soil was discretized into 1,455 solid hexahedron elements. The target plate included 2,639 hexahedron elements and was divided into four layers of elements along its 12.7-mm thickness in order to model bending. The loading plate included 1,152 hexahedron elements and was also divided into four layers of elements along its 25.4-mm thickness in order to model bending. The total number of nodes included in the finite element mesh was 7,169, and the total number of solid hexahedron elements was 5,474.

The soil behavior was simulated by the extended two invariant Cap model available in DYNA3D. A description of the two invariant Cap model can be found in Chen and Baladi (1985). For this preliminary analysis typical Cap parameter for a sand, similar to the one used in the

impulse tests, were utilized. The steel loading plate and the aluminum target plate were assumed to behave in a linear elastic manner with elastic moduli relevant to steel and aluminum, respectively.

The interface between the soil and different structural parts of the impulse test apparatus were carefully simulated utilizing the "sliding interface" available in DYNA3D. The sliding interface is a penalty-function based contact surface which allows sliding between disjoint model parts with separation and friction. Large relative motions are permitted, and Coulomb friction is included. Surfaces may separate and come together in a completely arbitrary fashion--a feature essential for the current analysis. A total of 1,458 interface facets were utilized in the current analysis. The soil/metal friction coefficient was assumed to be 0.43.

DYNA3D automatically calculates the maximum time step size, Δt, at each step of solution in its explicit central difference time scheme. The average time step size utilized in the current analysis was approximately 40 μs. This time step size was essentially the time required for an elastic stress wave to propagate across the shortest dimension of the smallest element in the finite element mesh.

The measured impulse load history for test 4, shown in Figure 5(d), was utilized as the input load applied to the loading plate. The calculated inward peak displacement of the loading plate, caused by the impulse load, was approximately 14 mm which is in good agreement with the measured inward peak displacement of approximately12 mm. The calculated peak strain of 43 $\mu\epsilon$ at the center of the target plate was also in good agreement with the 36 $\mu\epsilon$ that was measured at the same location (Figure 7b). This indicates that the assumed material properties for the sand are adequate. The calculated peak lateral earth pressure exerted on the target plate is shown in Figure

12. It is noted that the maximum earth pressures (normal stresses) are located at the center of the plate and also near the corners of the plate which were fixed to simulate actual test conditions.

CONCLUSION

The main objective of this study is to investigate the lateral propagation and attenuation of shock waves originating deep inside the soil in the vicinity of an underground protective structure, and the accompanying response of a subsection of the underground structure. A 1.0 m-high prototype subsection (termed target plate), was subjected to controlled impulsive loadings propagating through a 0.75.m-thick backfill soil. The response of the target plate to the impulsive loading was carefully measured utilizing an extensive instrumentation program.

Four impulse tests were conducted. Test results indicated that the measured peak strains in the target plate were the smallest in test 1 which was conducted under 35 kPa surcharge pressure and an impulse loading of 220 kPa. However, the measured peak strains in test 3, which was subjected to 105 kPa surcharge pressure and an impulse loading of 270 kPa, were considerably smaller than those of test 2, which was subjected to 70 kPa surcharge pressure and a smaller impulse loading of 250 kPa. This observation implies that the effect of impulse loading on the target plate is significantly influenced by the surcharge pressure.

The limited number of tests conducted during this study indicated that the damaging effect of impulse loading increased with surcharge pressure (depth) until a "threshold" surcharge pressure is reached above which the damaging effect of impulse loading decreased. This can be attributed to the increase of soil strength as the confining pressure increased. Apparently, this conclusion is based only on a limited number of tests, and further impulse tests with greater

impulse intensities, and with a variety of soil environments and conditions, are needed to ascertain the above observation.

Acknowledgment

The writers are grateful for support from U.S. Air Force Office of Scientific Research (Grant No. F49620-98-1-0109). The writers also thank Professor H-Y Ko from the University of Colorado-Boulder and Professor H. Tabatabai from the University of Wisconsin-Milwaukee for their comments and suggestions.

Table 1: Instrumentation

Instrument	Range	Frequency (Hertz)	Source
4 icp piezoelectric accelerometers	up to 50 g	1-10,000	PCB Piezotronics, Inc
4 icp piezoelectric accelerometers	up to 500 g	1-10.000	PCB Piezotronics, Inc
2 icp piezoelectric accelerometers	up to 10.000 g	1-10,000	PCB Piezotronics, Inc
11 piezoelectric strain gages	up to 1% strain	1-100,000	PCB Piezotronics, Inc
7 icp quartz interface press. sensors	up to 45 N	1-10,000	PCB Piezotronics, Inc
4 icp load cells (force sensors)	up to 45,000 N	1-10,000	PCB Piezotronics, Inc

Table 2: Impulse Test Designations

	Surcharge (kPa)	Measured Impulse Load History	Measured Impulse Acceleration at the Center of Loading Plate (g)
Test 1	35	Load History Fig. 5(a)	200
Test 2	70	Load History Fig. 5(b)	240
Test 3	105	Load History Fig. 5(c)	560
Test 4	70	Load History Fig. 5(d)	680, see Figure 6(a)

Table 3: Measured P-Wave Velocities and Elastic Moduli

	Surcharge (kPa)	Measured v_p (m/s)	Calculated Initial G (kPa)	ν (assumed)
Test 1	35	222	27,372	0.25
Test 2	70	241.8	32,440	0.25
Test 3	105	246.8	33,805	0.25
Test 4	70	229	29,075	0.25

REFERENCES

Albritton, G. E. (1968). "Behavior of Flexible Cylinders Buried in Sand under Static and Dynamic Loading." Technical Report 1-821, U.S. Army Waterways Experiment Station, Vicksburg, Mississippi.

Allgood, J.R. (1970). "Structures in Soil under High Loads." ASCE Conference, Portland, Oregon, April.

Balsara, J.P. and Cummins, R.S., Jr. (1968). "Pressure Distribution on a Buried Flat Plate Subjected to Static and Airblast Overpressures." Misc. Paper N-68-4, U.S. Army Waterways Experiment Station, Vicksburg, Mississippi.

Chen, H.L., and Chen, S.E. (1996). "Dynamic Responses of Shallow-Buried Flexible Plates Subjected to Impact Loading." *ASCE Journal of Structural Engineering*, Vol. 122, No. 1, pp. 55-60.

Chen, H.L., Shah, S.P., and Keer, L.M. (1990). "Dynamic Response of Shallow-Buried Cylindrical Structures." *J. Engrg. Mech. Div.*, ASCE, 116(1), 152-171.

Chen, W.F., and Baladi, G.Y., Soil Plasticity: Theory and Implementation, Elsevier, New York, 1985.

Gere, J.M., and H.C. Shah. 1984. Terra Nonfirma. *Understanding and Preparing for Earthquakes*. W.H. Freeman and Co., New York, NY.

Getchell, J.V., Kiger, S.A., Slawson, T.R., and Hyde, D.W. (1984). "Vulnerability of Shallow-Buried Flat-Roof Structures." Tech. Rep. Sl-80-7, U.S. Army Engineers Waterways Experiment Station, Vicksburg, Miss.

Ghaboussi, J., Millavec, W.A., and Isenberg, J. (1984) "R/C Structures Under Impulse Loading." *Journal of Structural Engineering*, ASCE, Vol. 110, No. 3, pp. 505-522.

Gill, H.L. (1967). "Active Arching of Sand during Dynamic Loading." Tech. Rep. R541, U.S. Naval Civ. Engrg. Lab., Port Hueneme, Calif.

Hallquist, J.O. (1982). "Theoretical Manual for DYNA3D." *University of California*, Lawrence Livermore National Laboratory, Report UCID-19401

Ko, H-Y (1988). "Summary of the State-of-the-Art in Centrifuge Model Testing." *Centrifuge in Soil Mechanics*; Craig, James, and Schofield (editors), Balkema, Rotterdam.

Ko, H-Y (1994). "Modeling Seismic Problems in Centrifuges." *Centrifuge 94*; Leung, Lee, and Tan (editors), Balkema, Rotterdam.

Kolbuszewski, J.J. (1948). "General Investigation of the Fundamental Factors Controlling Loose Packing of Sands." Proc., Second International Conference on Soil Mechanics and Foundation Engineering, Rotterdam.

Palacios, N. and Kennedy, T.E. (1967). "The Dynamic Response of Buried Concrete Arches, Project 3.2, Operation Snowball." Tech. Report 1-797, U.S. Army Engineer Waterways Experiment Station, Vicksburg, Mississippi.

Puglisi, R.D., and Krauthammer, K. (1987). "Dynamic Response Analysis of Shallow-Buried Reinforced Concrete Arches." Civil and Mineral Engineering Report ST-87-06, University of Minnesota, Minneapolis, Minnesota.

Schofield, A.N. (1988). "An Introduction to Centrifuge Modeling." *Centrifuge in Soil Mechanics*; Craig, James, and Schofield (editors), Balkema, Rotterdam.

Shim, H-S (1995). "Response of Piles in Saturated Soil under Blast Loading." Thesis presented to the University of Colorado in partial fulfillment of the requirements for the degree of Doctor of Philosophy. The University of Colorado at Boulder, December, 1995.

Slawson, T.R. (1984). "Dynamic Shear Failure of Shallow-Buried Flat-Roofed Reinforced Concrete Structure Subjected to Blast Loading." Final Rep. SL-84-7, U.S. Army Engineers Waterways Experiment Station, Vicksburg, Miss.

Vortman, L.J. (1979). "Prediction of Ground Motion from Nuclear Weapon Tests at NTS," Report SAND 79-1002. Sandia National Laboratories. Albuquerque, NM.

Vortman, L.J. (1981). "A Comparison of Ground Motion from Earthquakes and Underground Nuclear Weapons Tests at NTS". Workshop on Seismic Performance of Underground Facilities. Augusta, GA.

Weidlinger, P., and Hinman, E. (1988). "Analysis of Underground Protective Structures." *J. Struct. Engrg. Div.*, ASCE, 114(7), 1658-1672

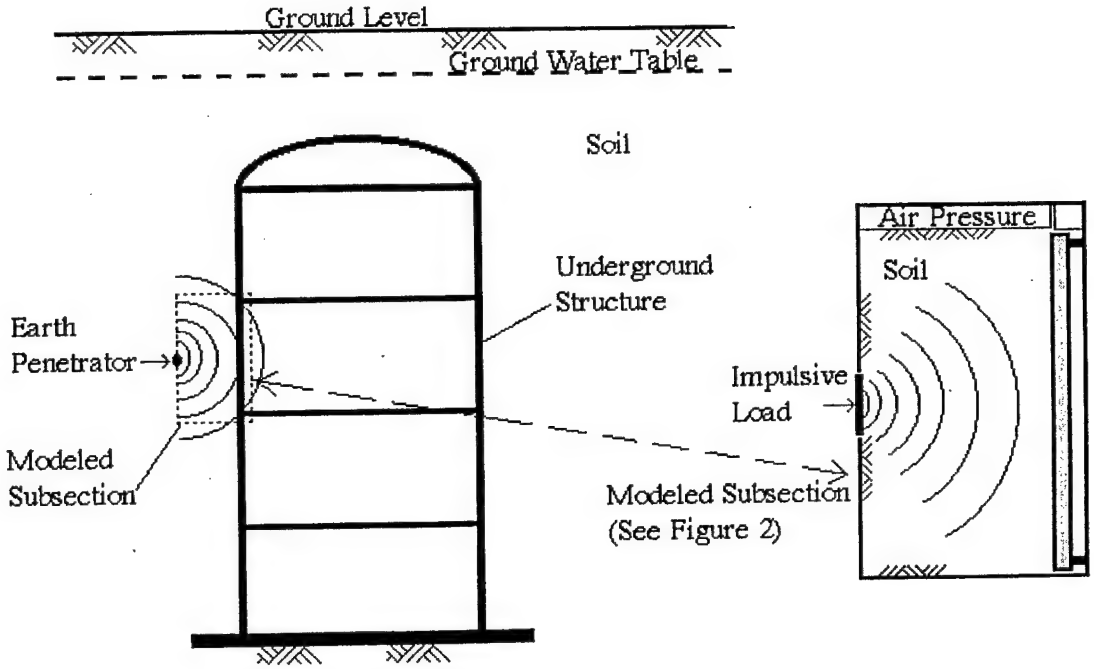

Figure 1: Concept of the Large-Scale Impulse Test

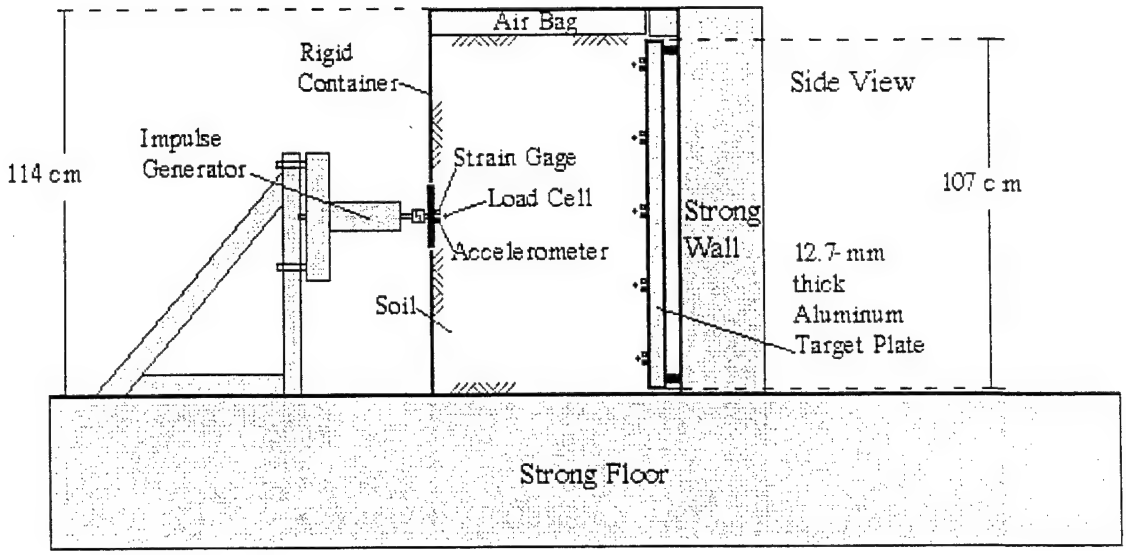

Figure 2: Configuration of the Large-Scale Impulse Test

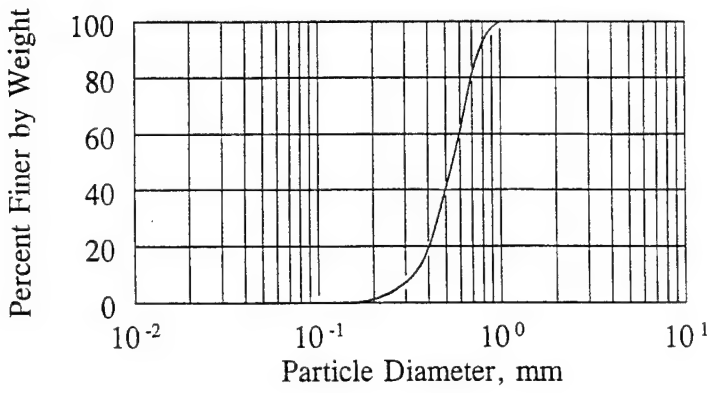

Figure 3: Particle Size Distribution Curve for Sand

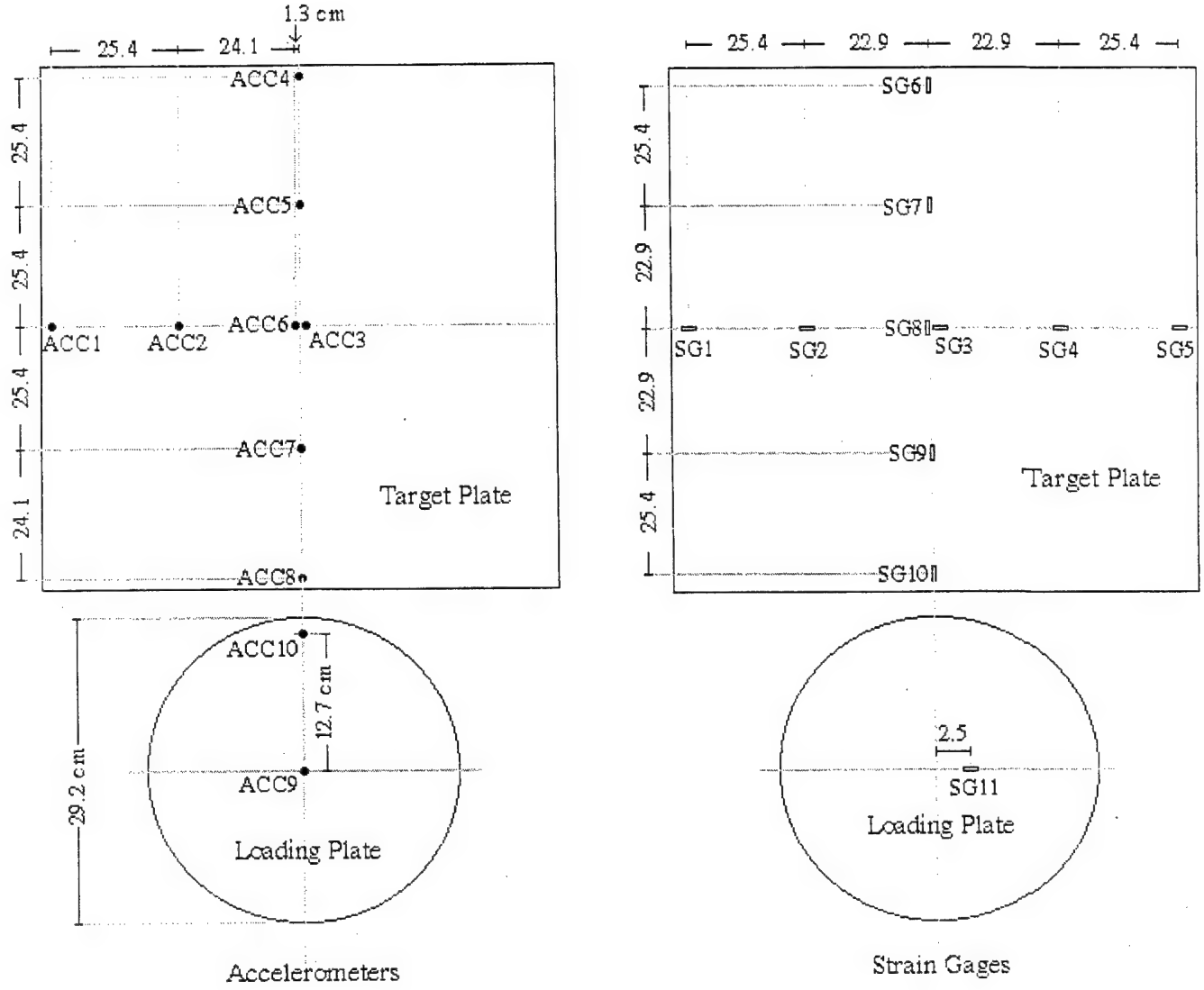

Figure 4: Instrumentation Program

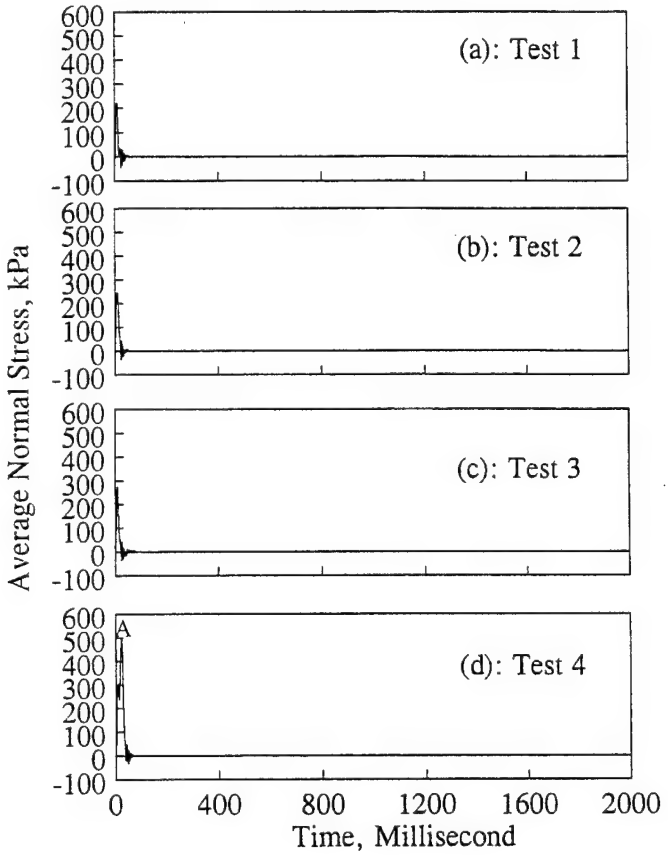

Figure 5: Impulse Load Histories for Tests 1, 2, 3, and 4

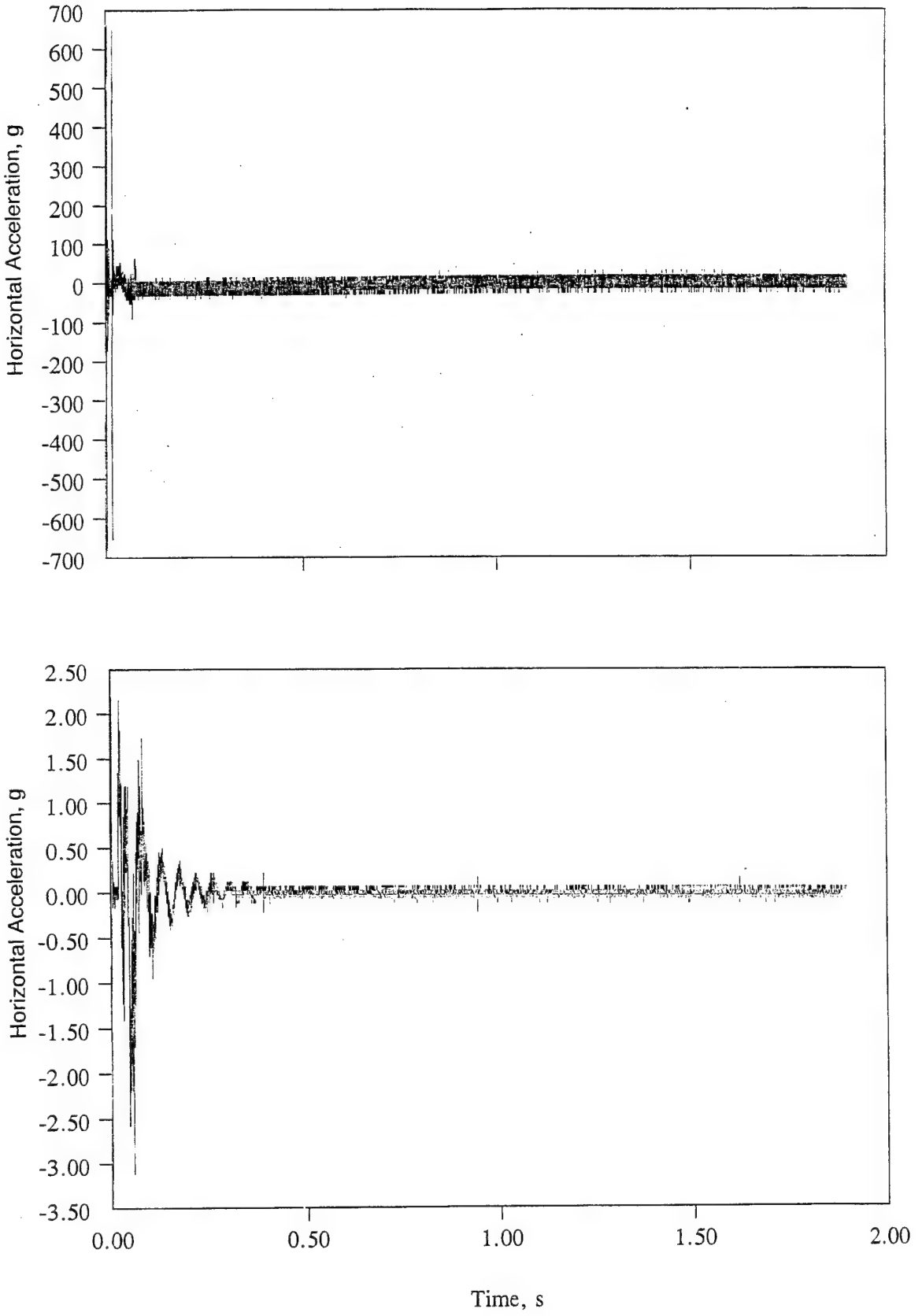

Figure 6: Acceleration History (a) at the Center of the Loading Plate (ACC9), and (b) at the Center of the Target Plate (ACC3)

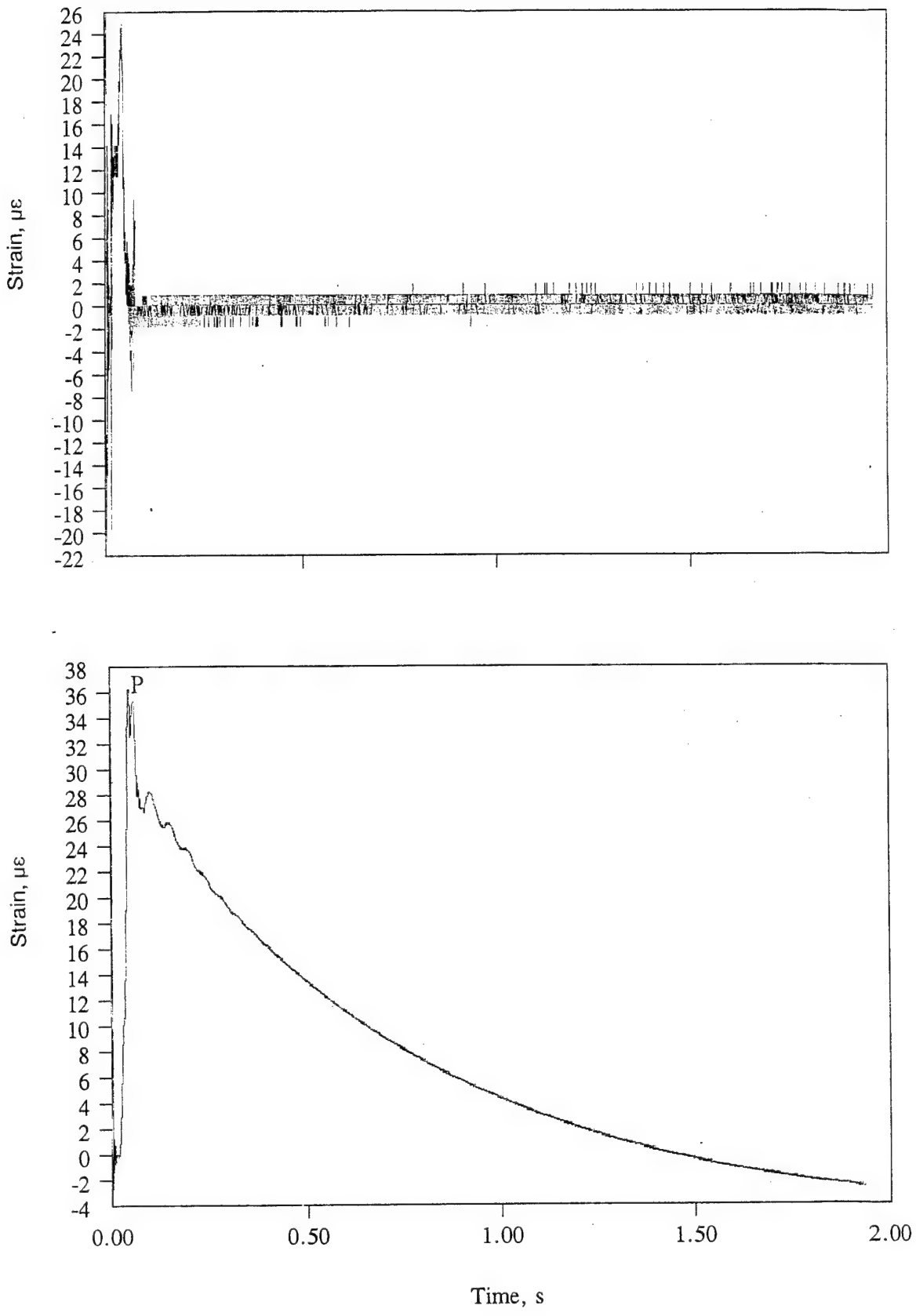

Figure 7: Strain History (a) at the Center of the Loading Plate (SG11), and (b) at the Center of the Target Plate (SG3)

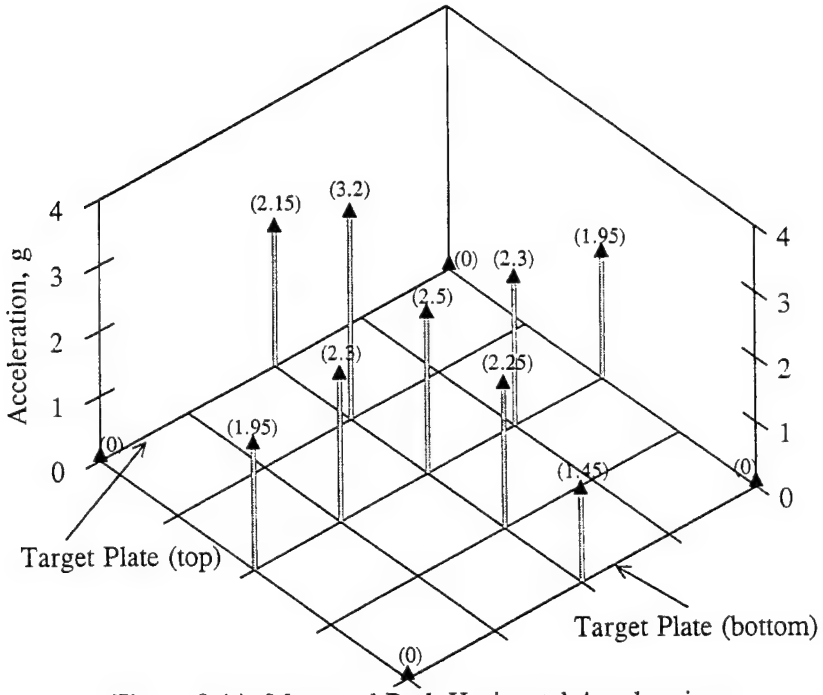

Figure 8 (a): Measured Peak Horizontal Accelerations on Target Plate (Test 4)

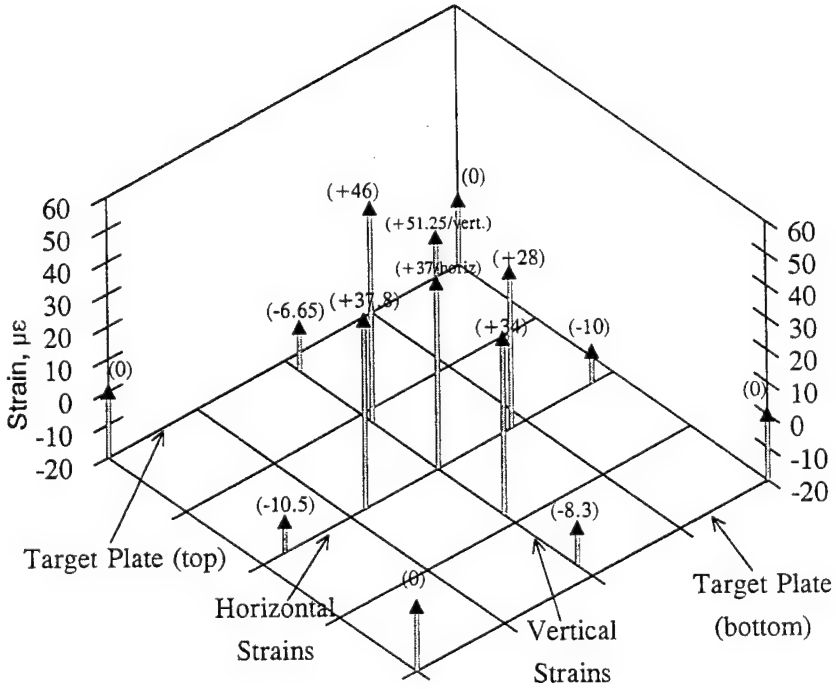

Figure 8 (b): Measured Peak Strains on Target Plate (Test 4)

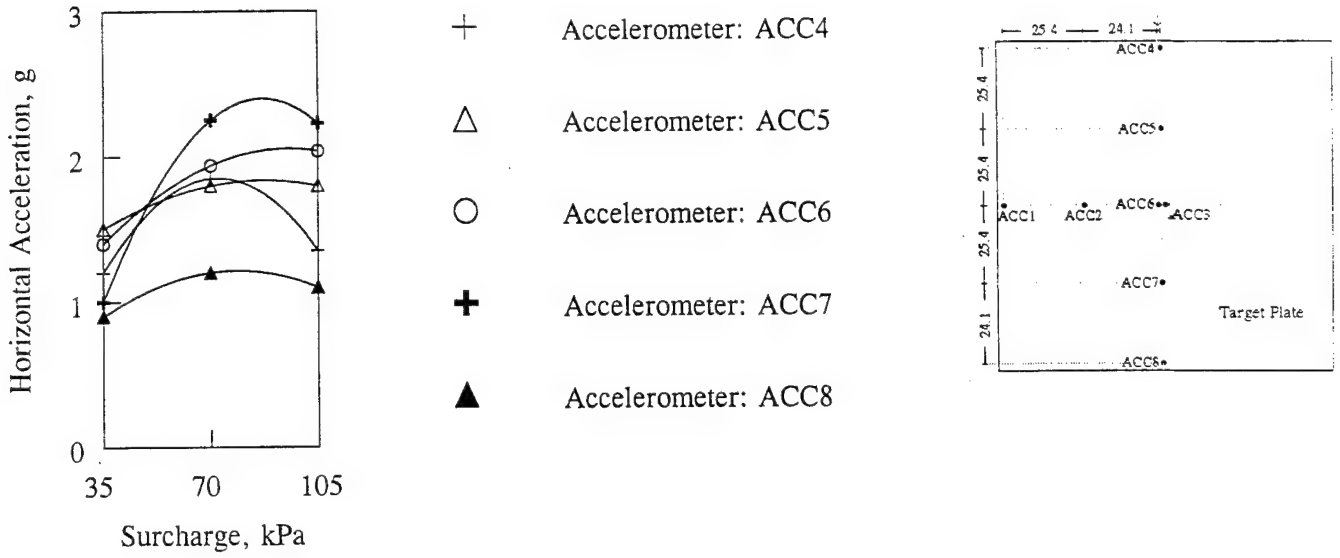

Figure 9(a): Comparison of Measured Horizontal Accelerations on Target Plate for Tests 1, 2, and 3

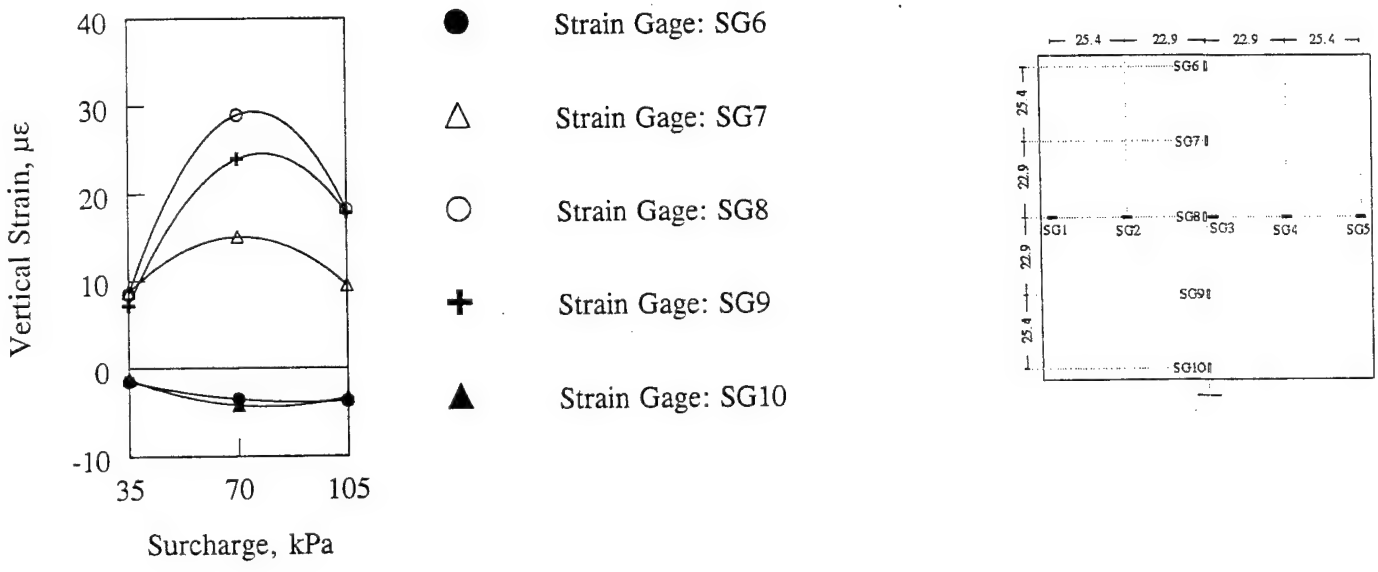

Figure 9(b): Comparison of Measured Peak Strains on Target Plate for Tests 1, 2, and 3

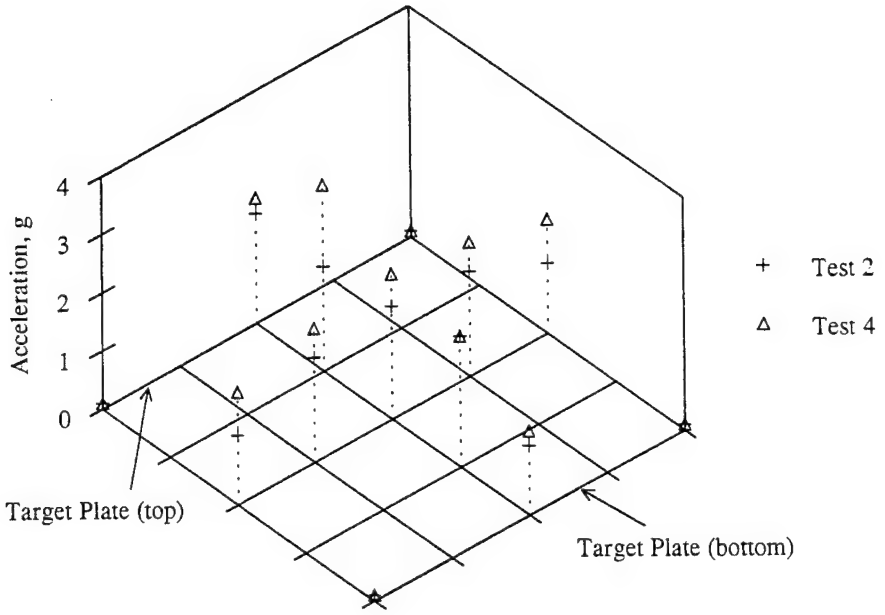

Figure 10 (a): Comparison between Measured Peak Horizontal Accelerations on Target Plate for Tests 2 and 4

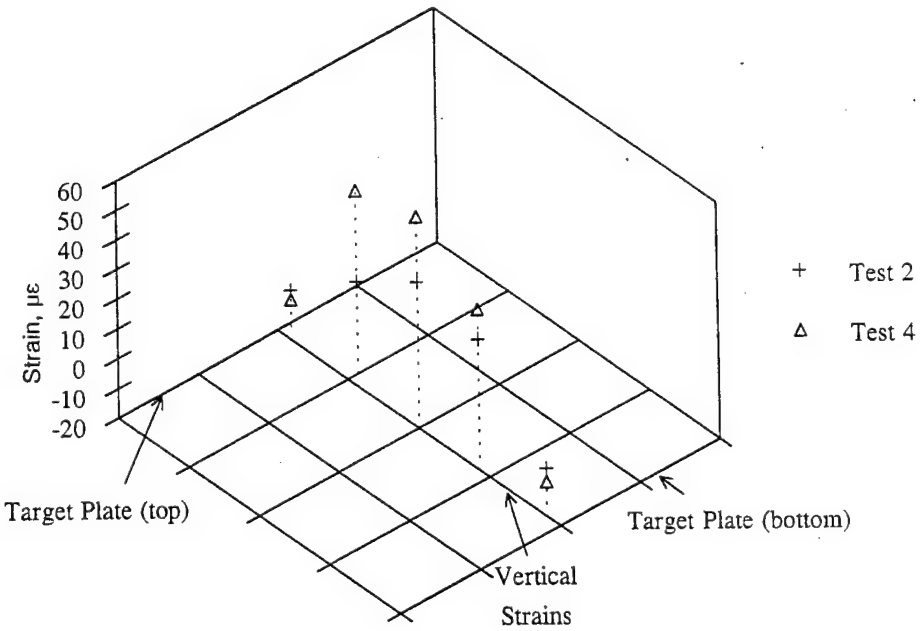

Figure 10(b) : Comparison of Measured Peak Strains on Target Plate for Tests 2 and 4

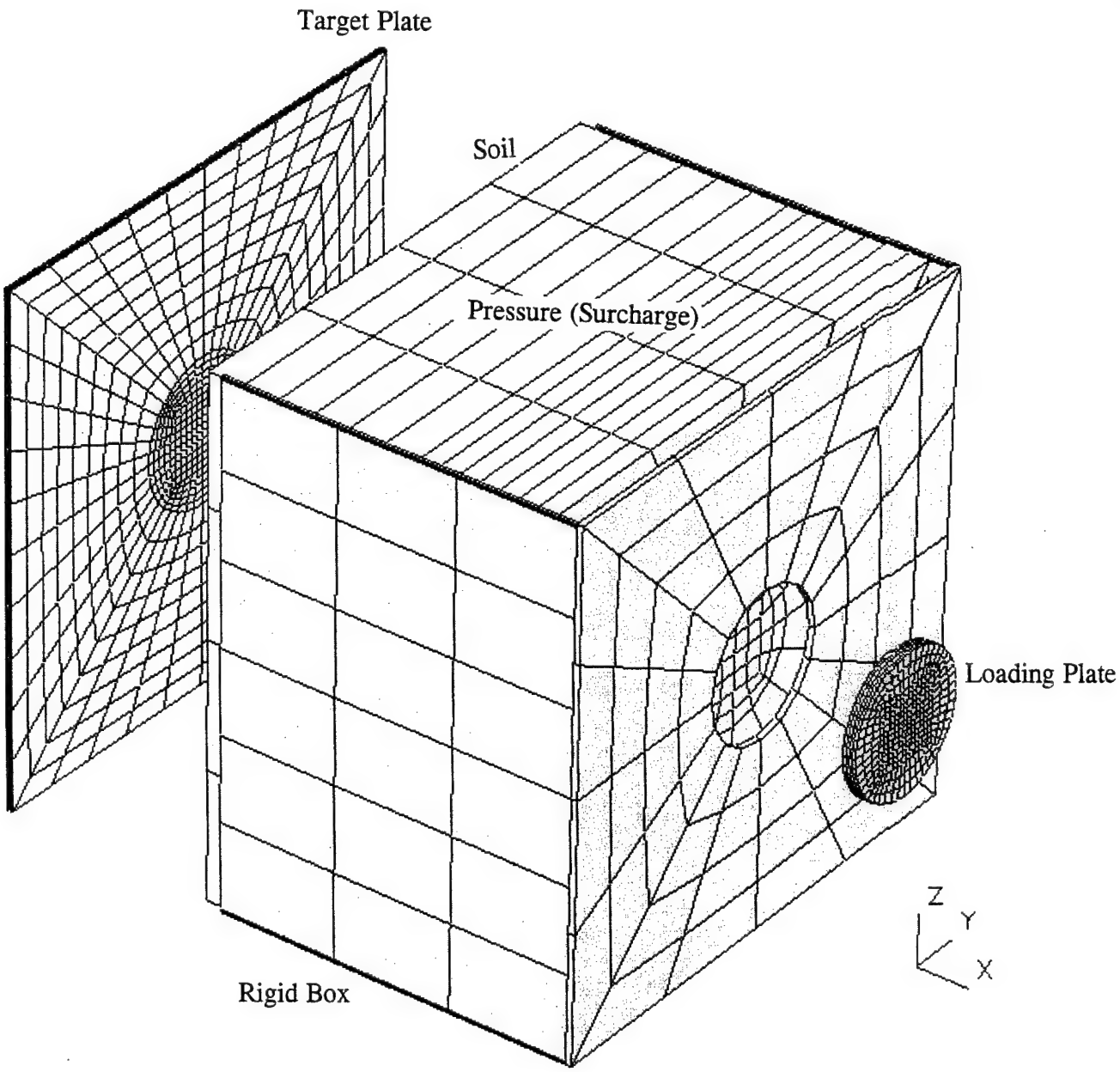

Figure 11: Finite Element Discretization (Exploded) of the Large-Scale Impulse Test

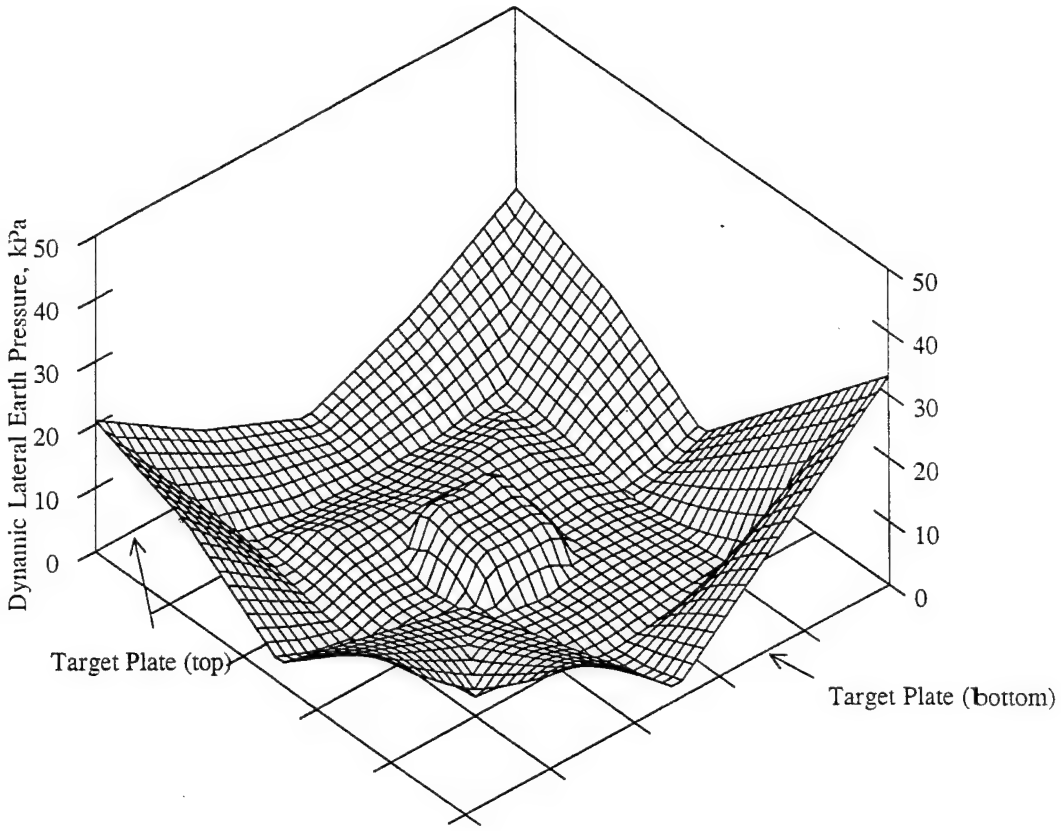

Figure 12: Calculated Dynamic Lateral Earth Pressure on Target Plate at t= 25.47 ms

APPENDIX A

Detailed Measurement for Test 4

File Name	DAQ_CARD #	DAQ_CHANNEL	GLOBAL CHANNEL	SCALINING_FACTOR
D:\Program Files\National Instruments\LabVIEW\sam4_5	5	7	32	9.50600

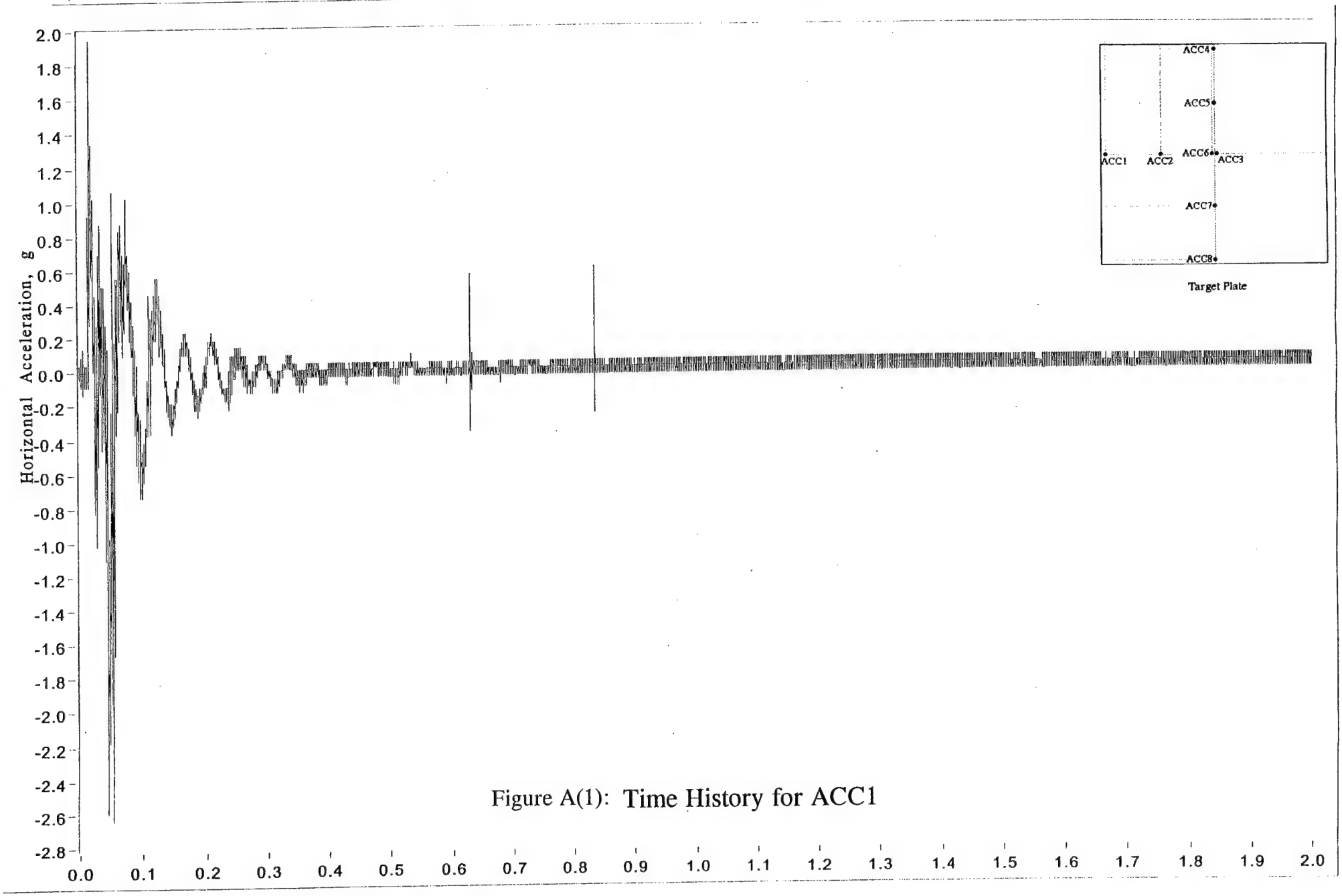

Figure A(1): Time History for ACC1

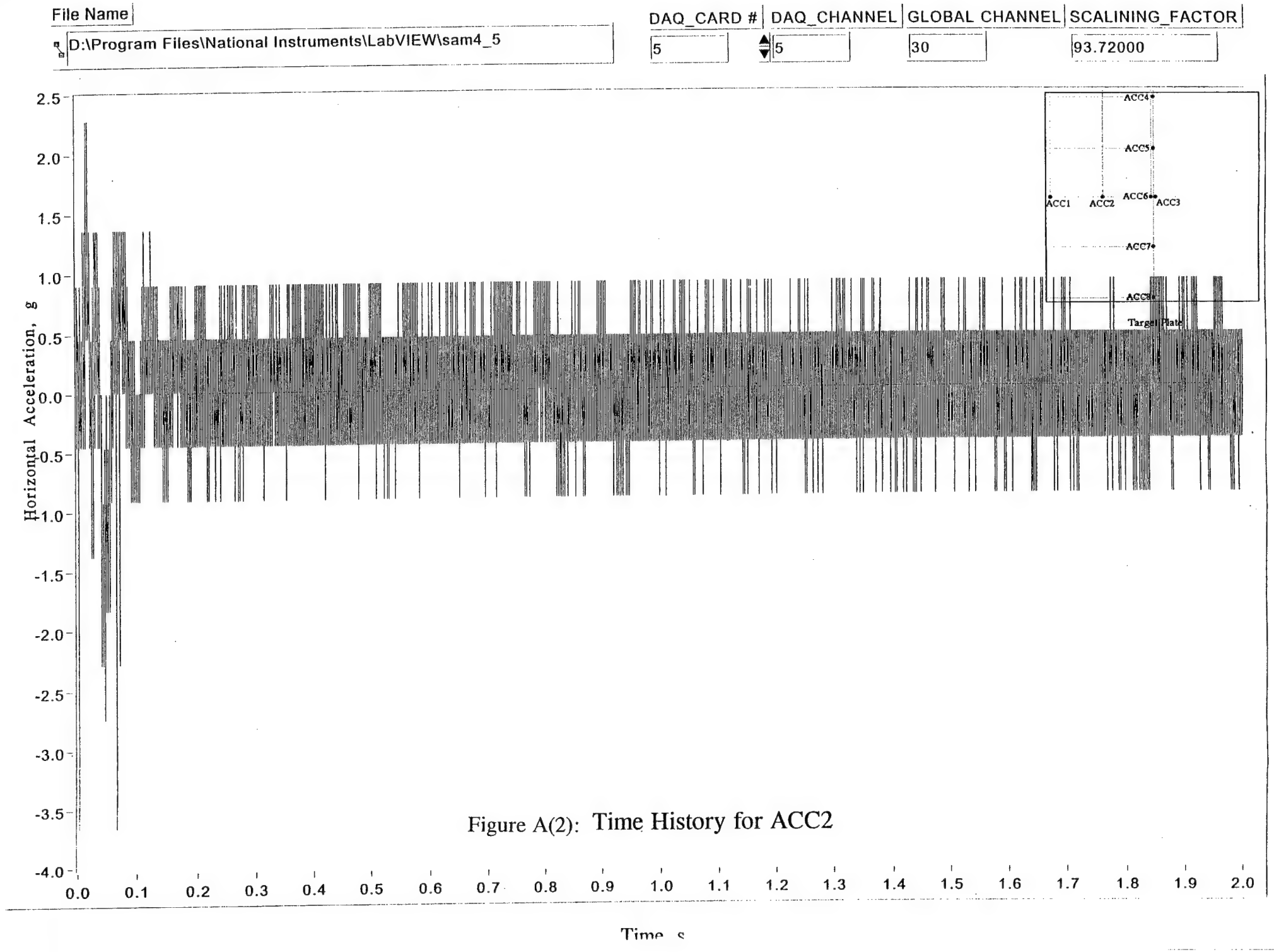

Figure A(2): Time History for ACC2

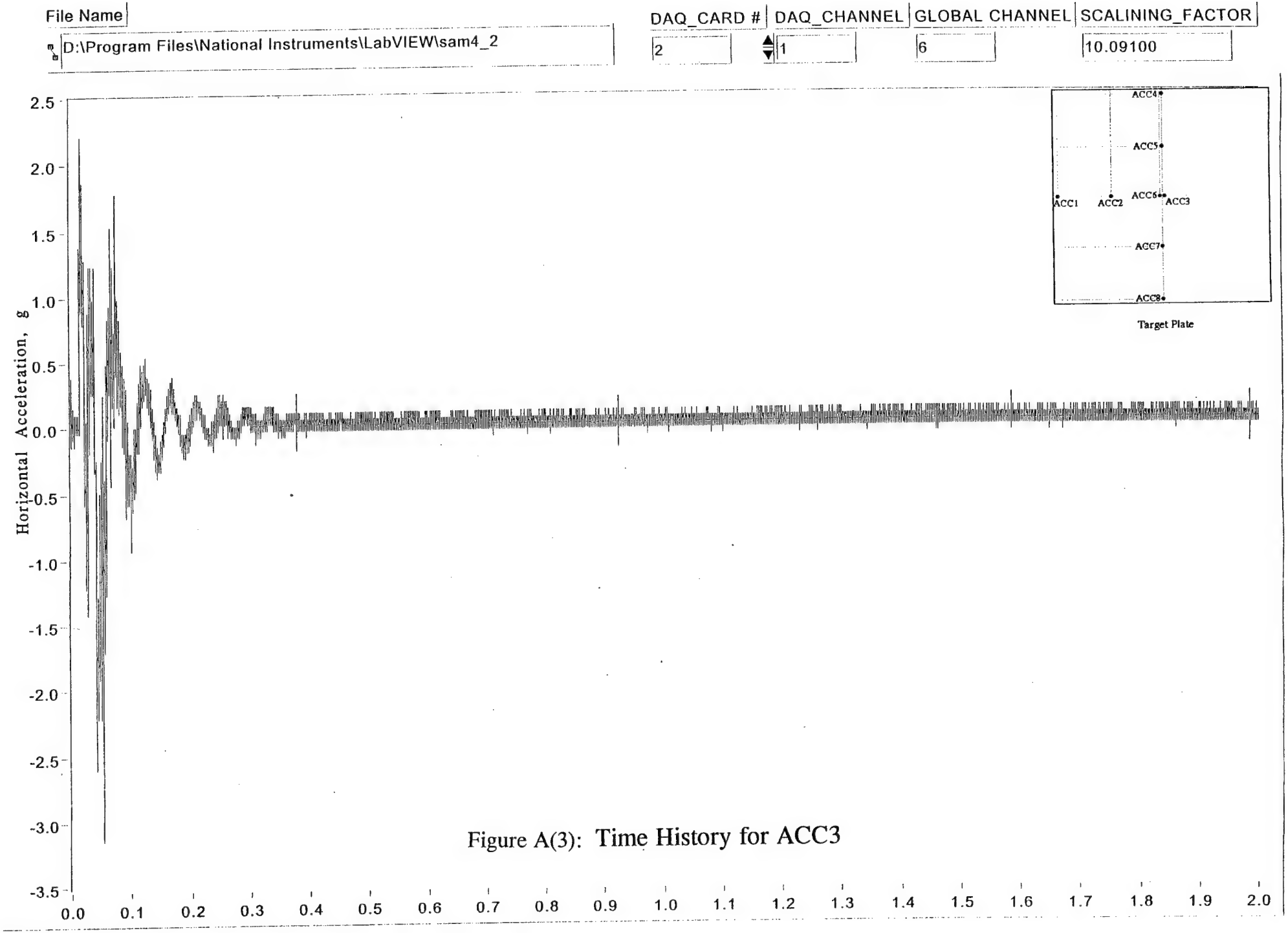

Figure A(3): Time History for ACC3

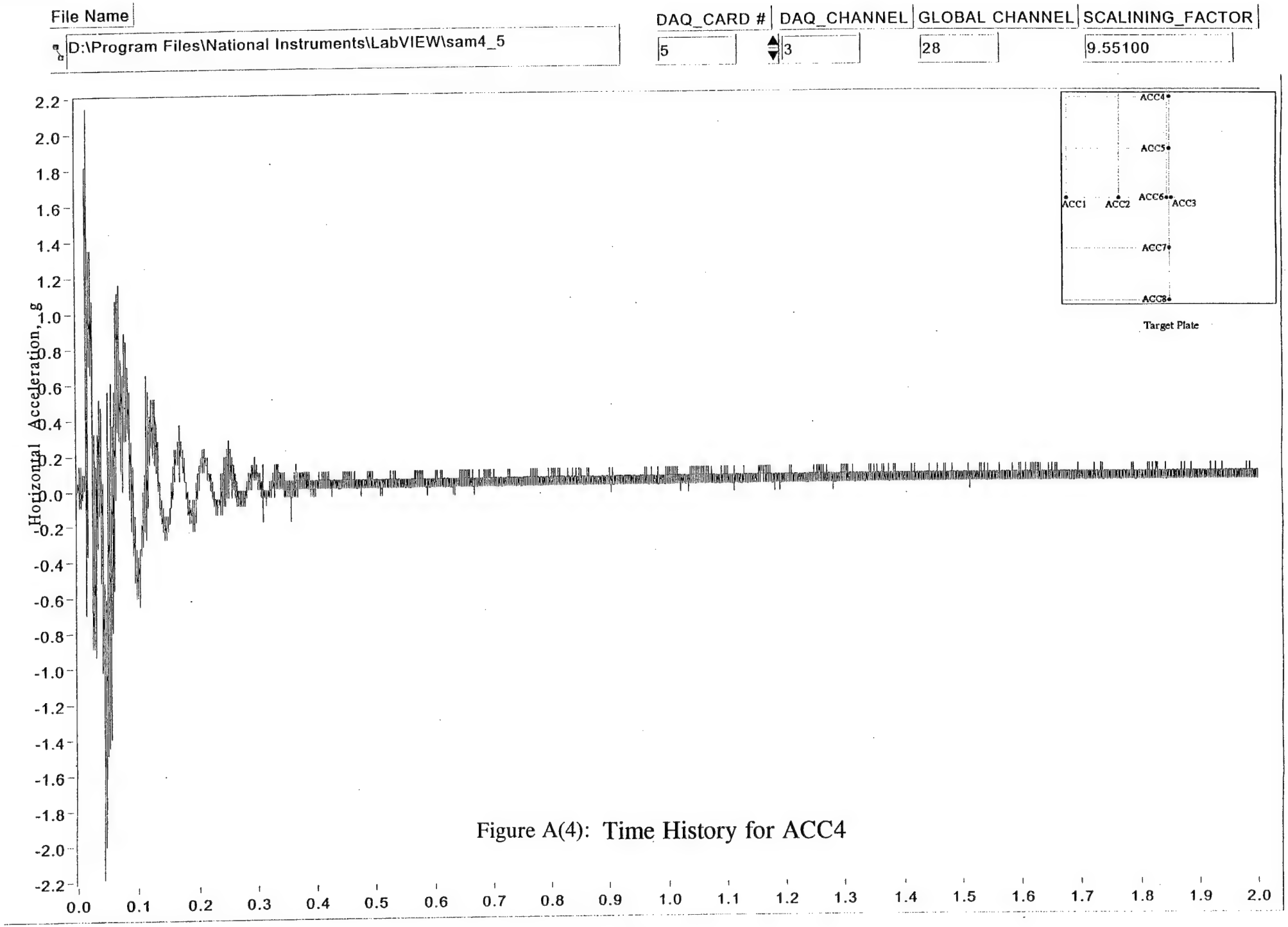

Figure A(4): Time History for ACC4

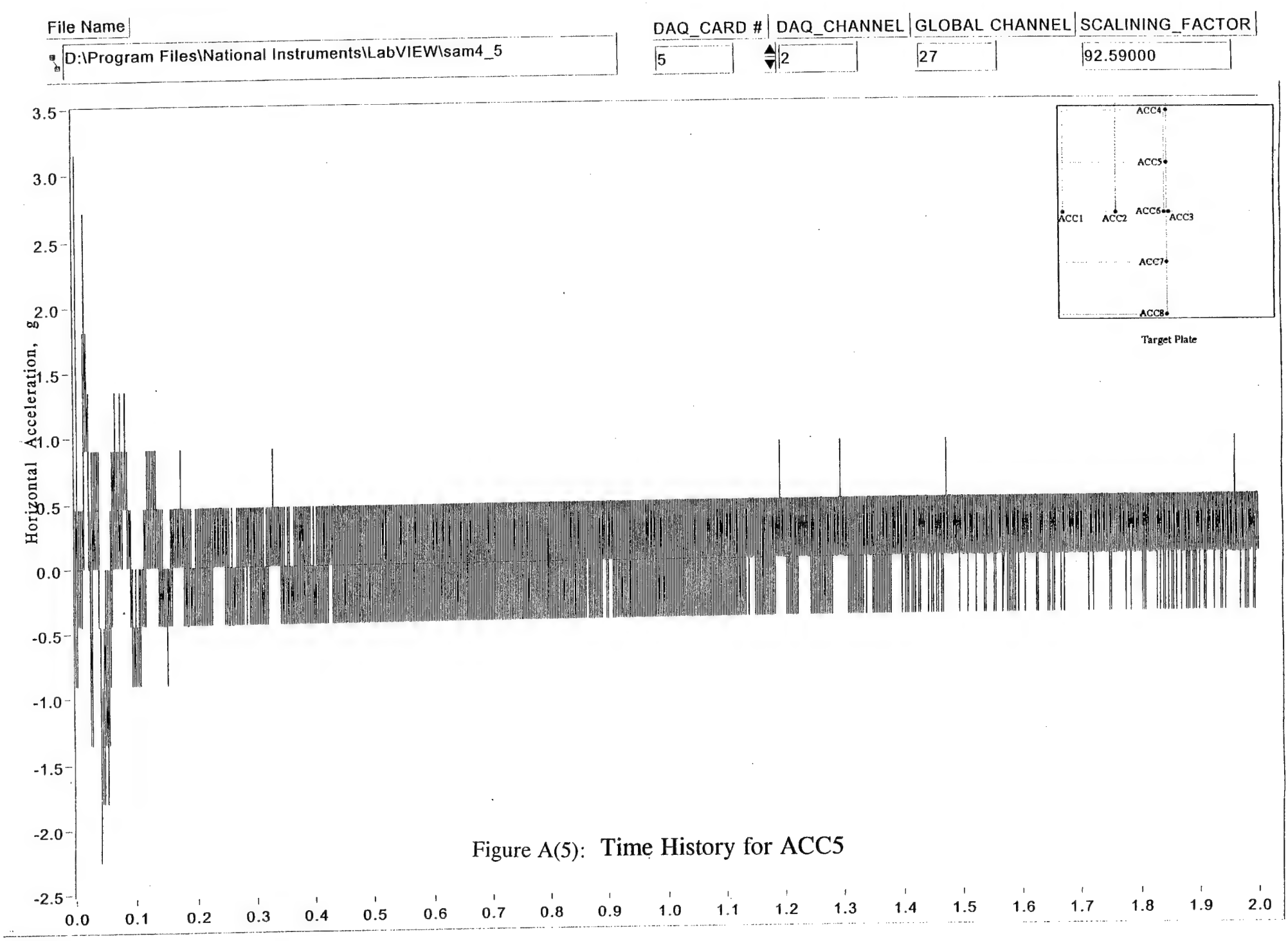

Figure A(5): Time History for ACC5

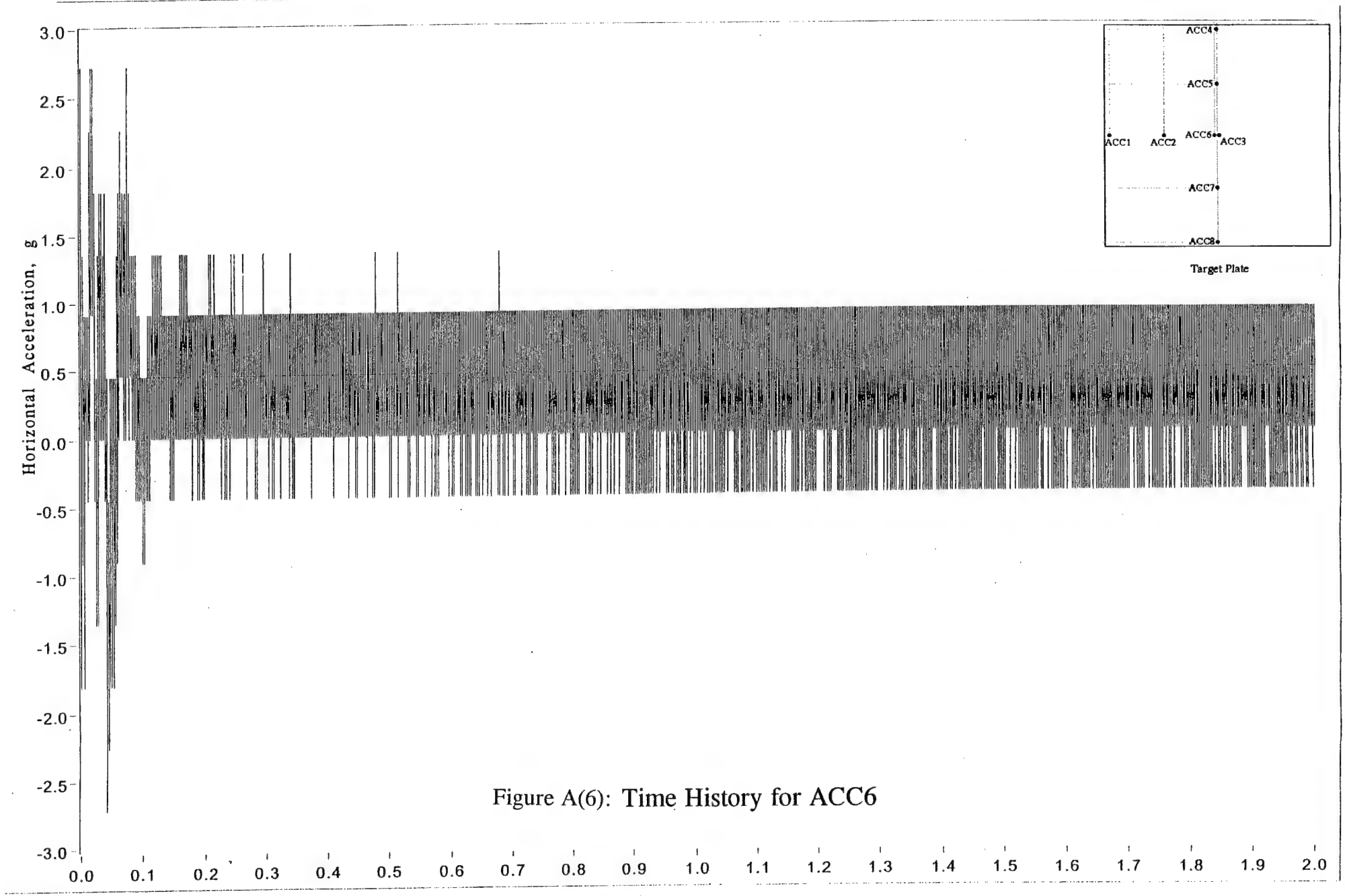

Figure A(6): Time History for ACC6

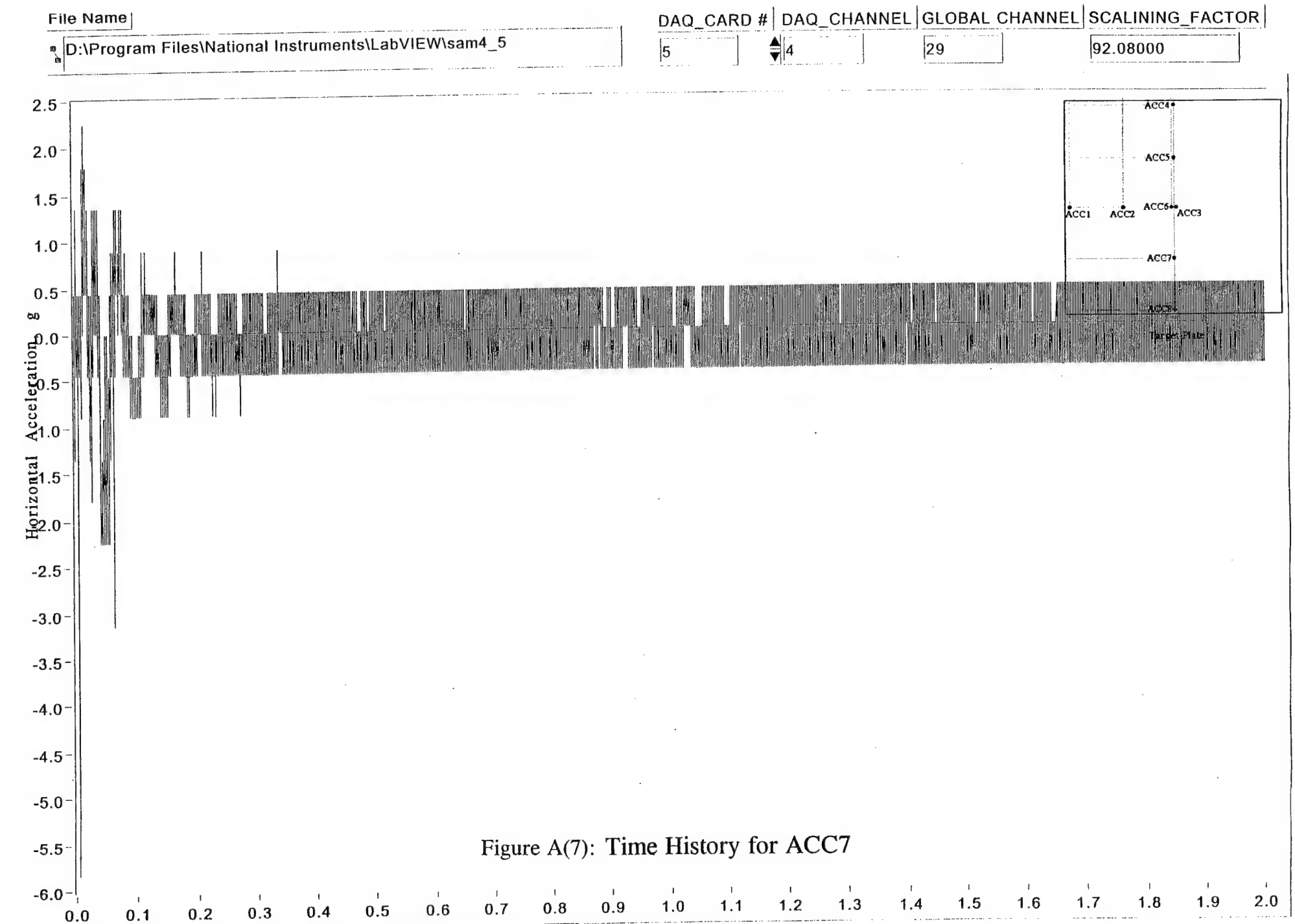

Figure A(7): Time History for ACC7

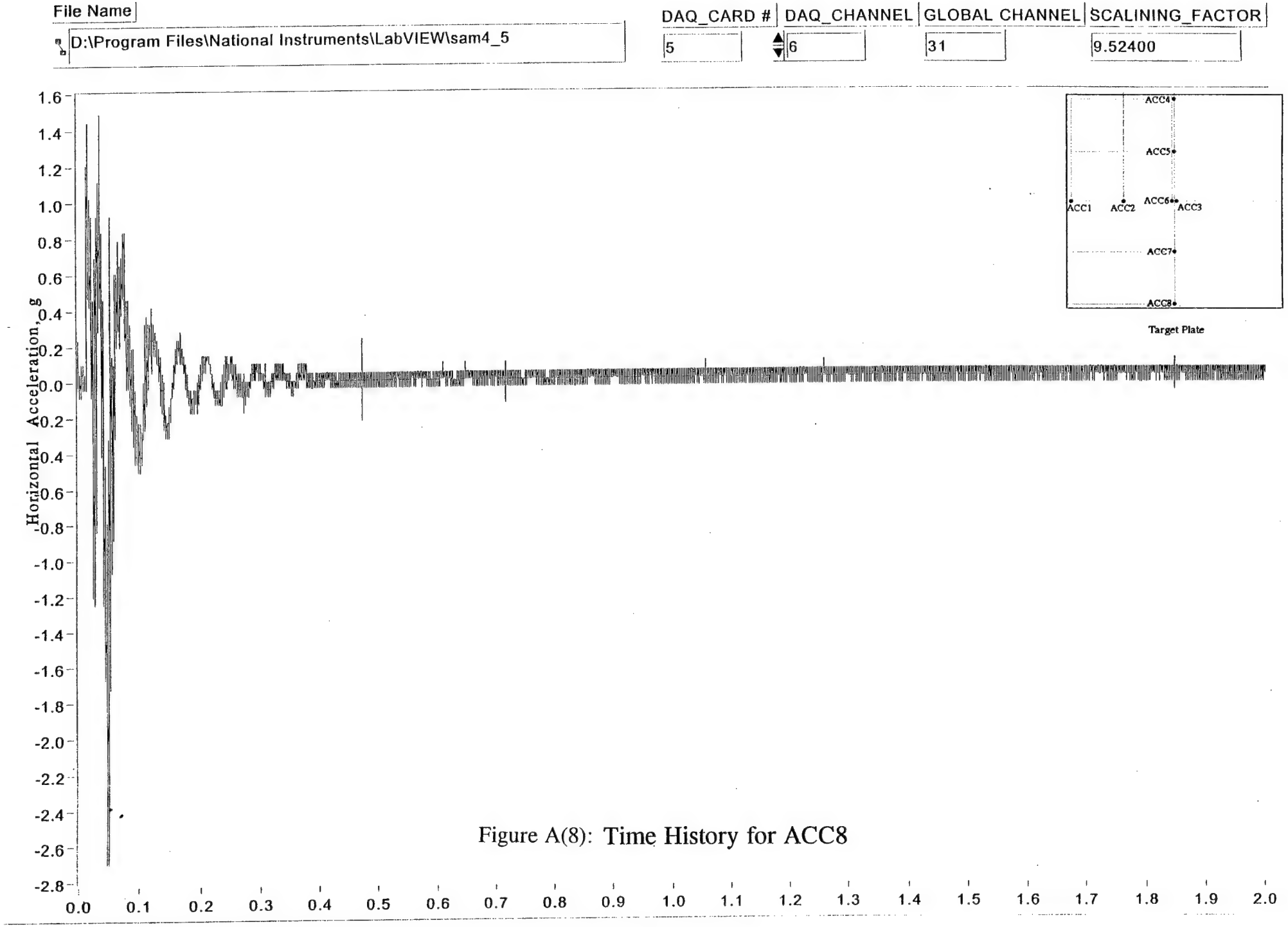

Figure A(8): Time History for ACC8

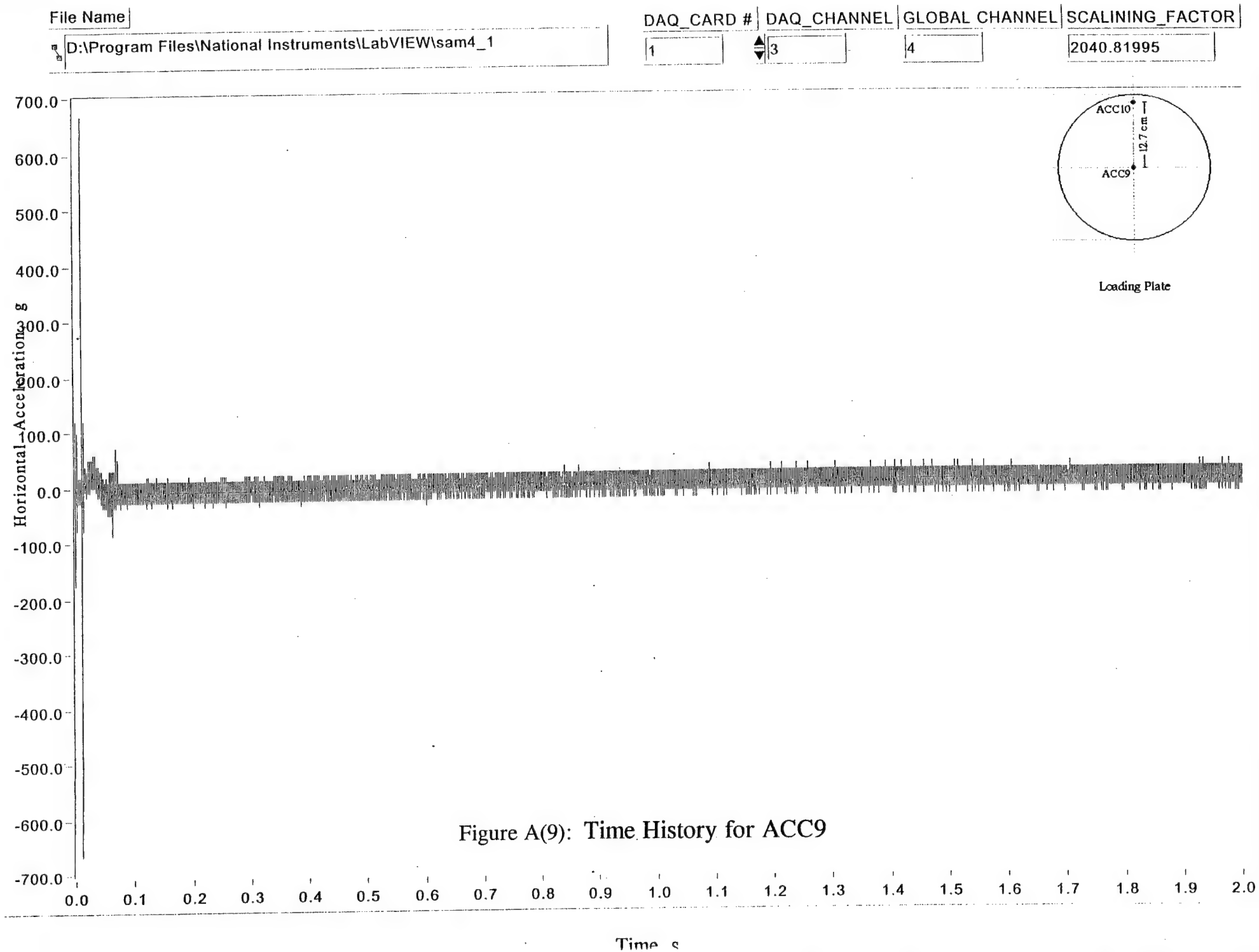

Figure A(9): Time History for ACC9

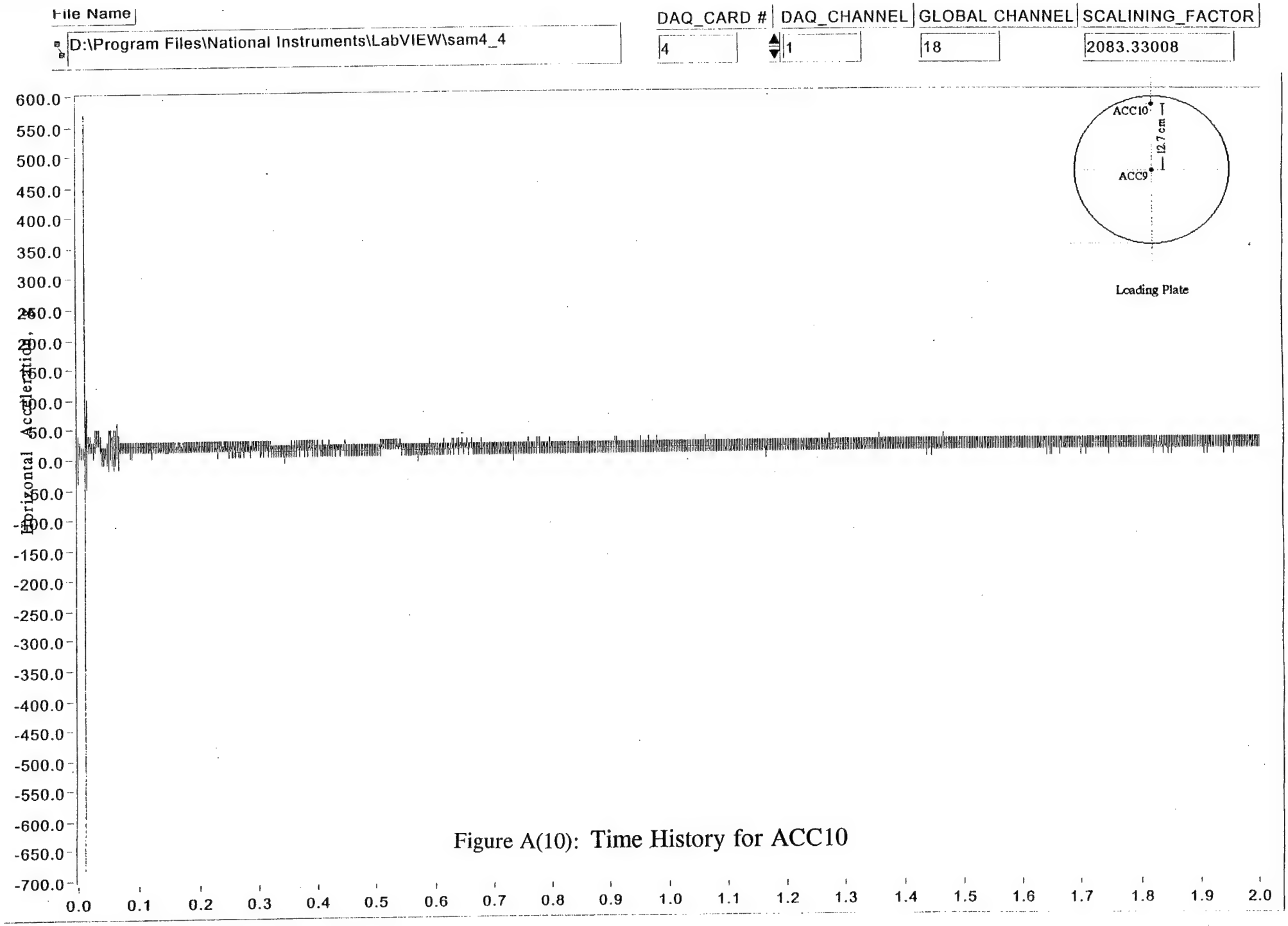

Figure A(10): Time History for ACC10

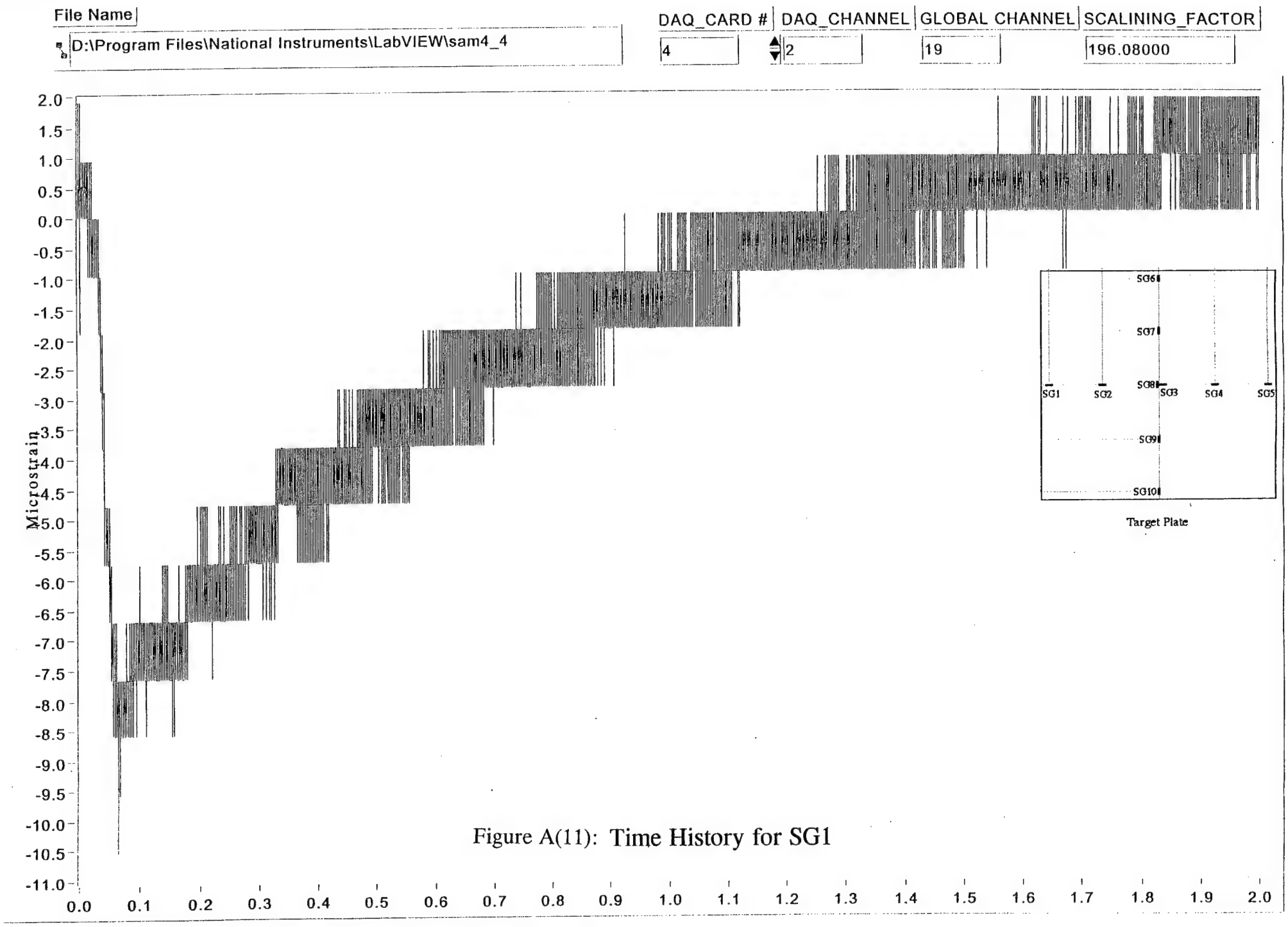

Figure A(11): Time History for SG1

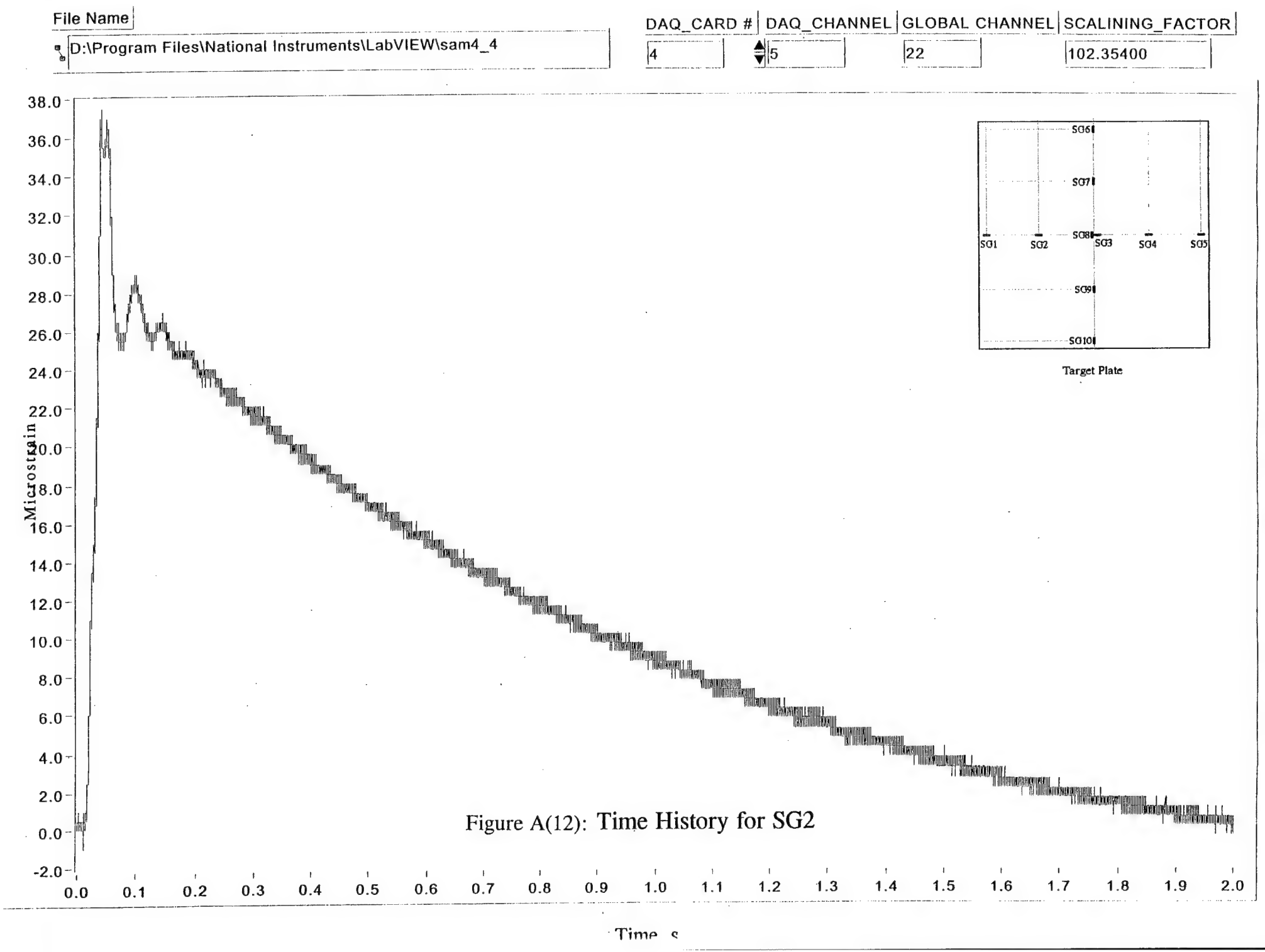

Figure A(12): Time History for SG2

File Name

D:\Program Files\National Instruments\LabVIEW\sam4_1

DAQ_CARD #	DAQ_CHANNEL	GLOBAL CHANNEL	SCALINING_FACTOR
1	1	2	19.53100

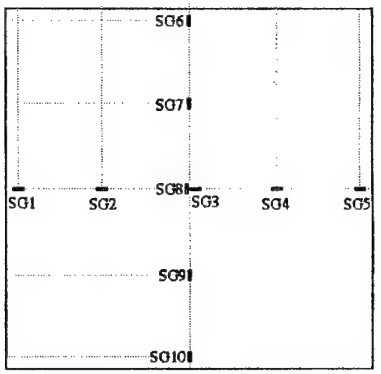

Target Plate

Microstrain

38.0
36.0
34.0
32.0
30.0
28.0
26.0
24.0
22.0
20.0
18.0
16.0
14.0
12.0
10.0
8.0
6.0
4.0
2.0
0.0
-2.0
-4.0

0.0 0.1 0.2 0.3 0.4 0.5 0.6 0.7 0.8 0.9 1.0 1.1 1.2 1.3 1.4 1.5 1.6 1.7 1.8 1.9 2.0

Time, s

Figure A(13): Time History for SG3

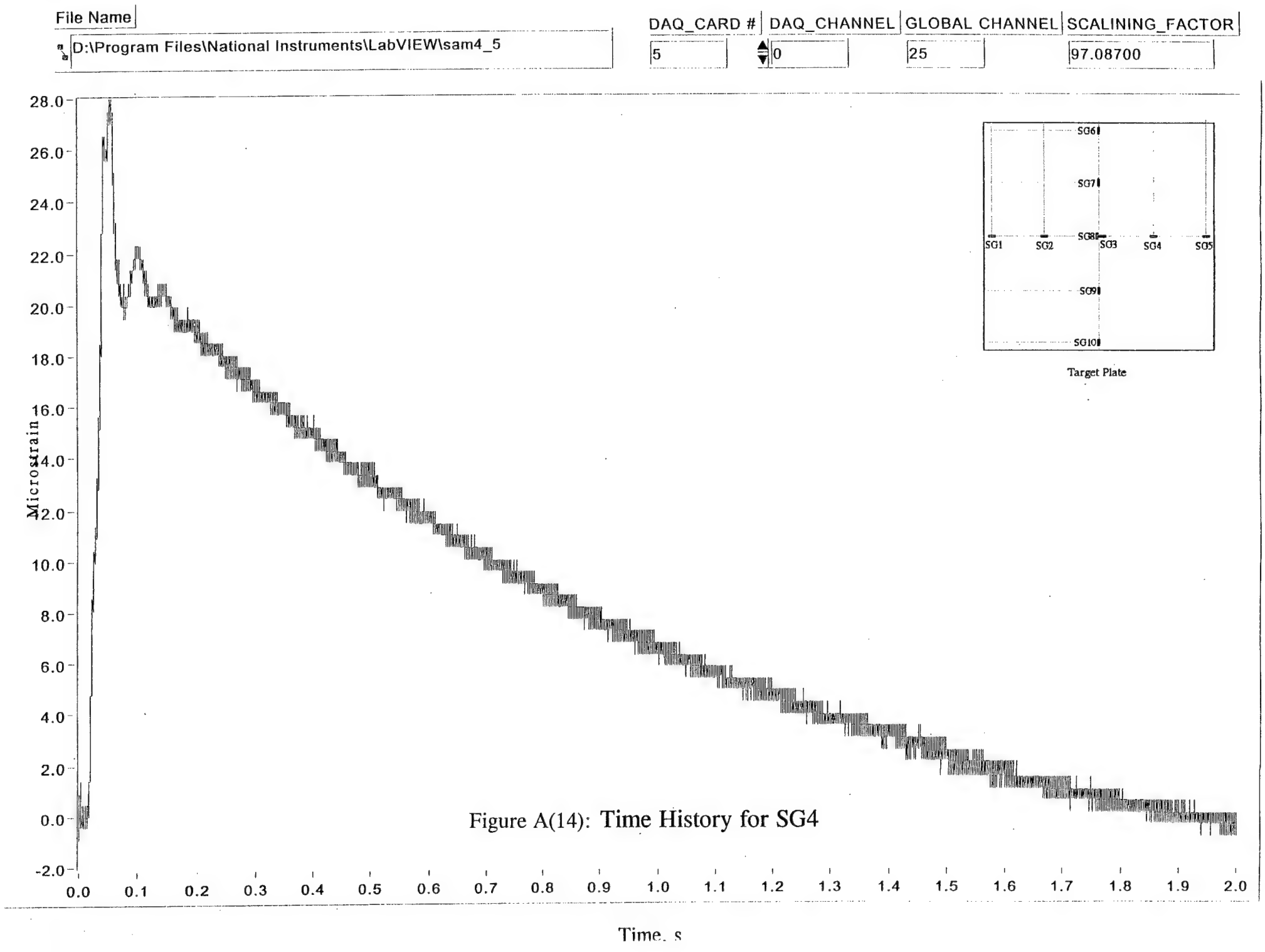

Figure A(14): Time History for SG4

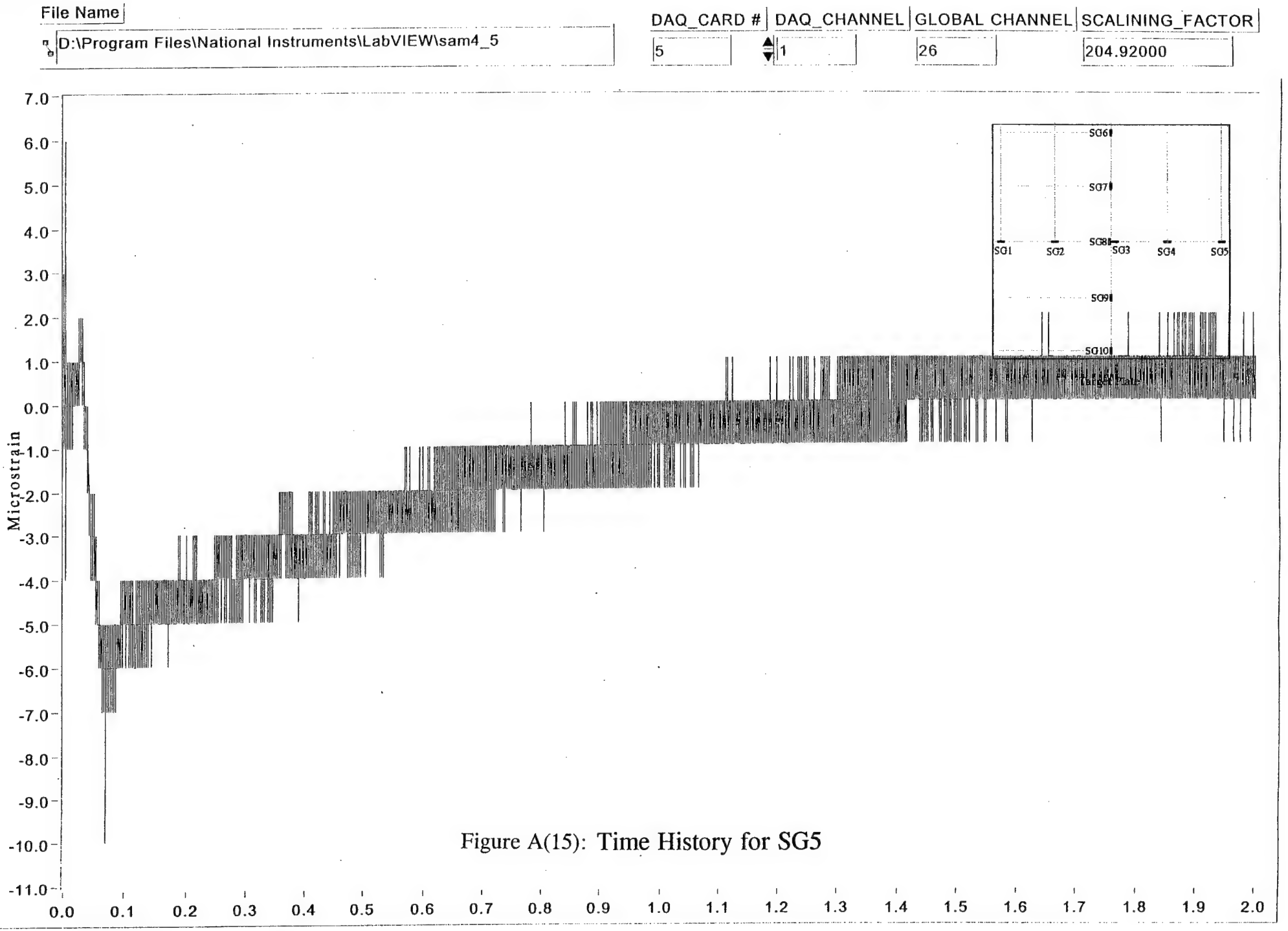

Figure A(15): Time History for SG5

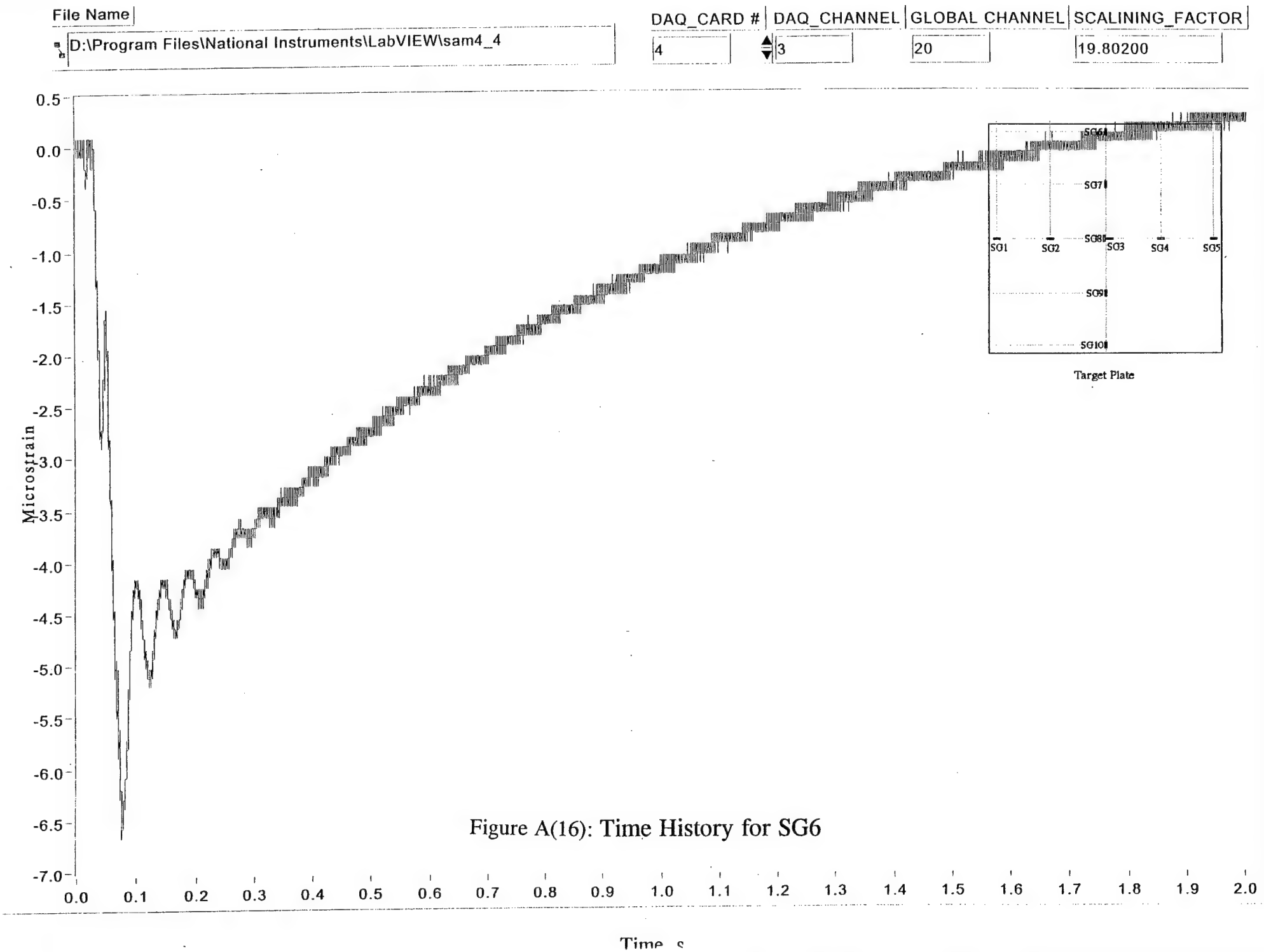

Figure A(16): Time History for SG6

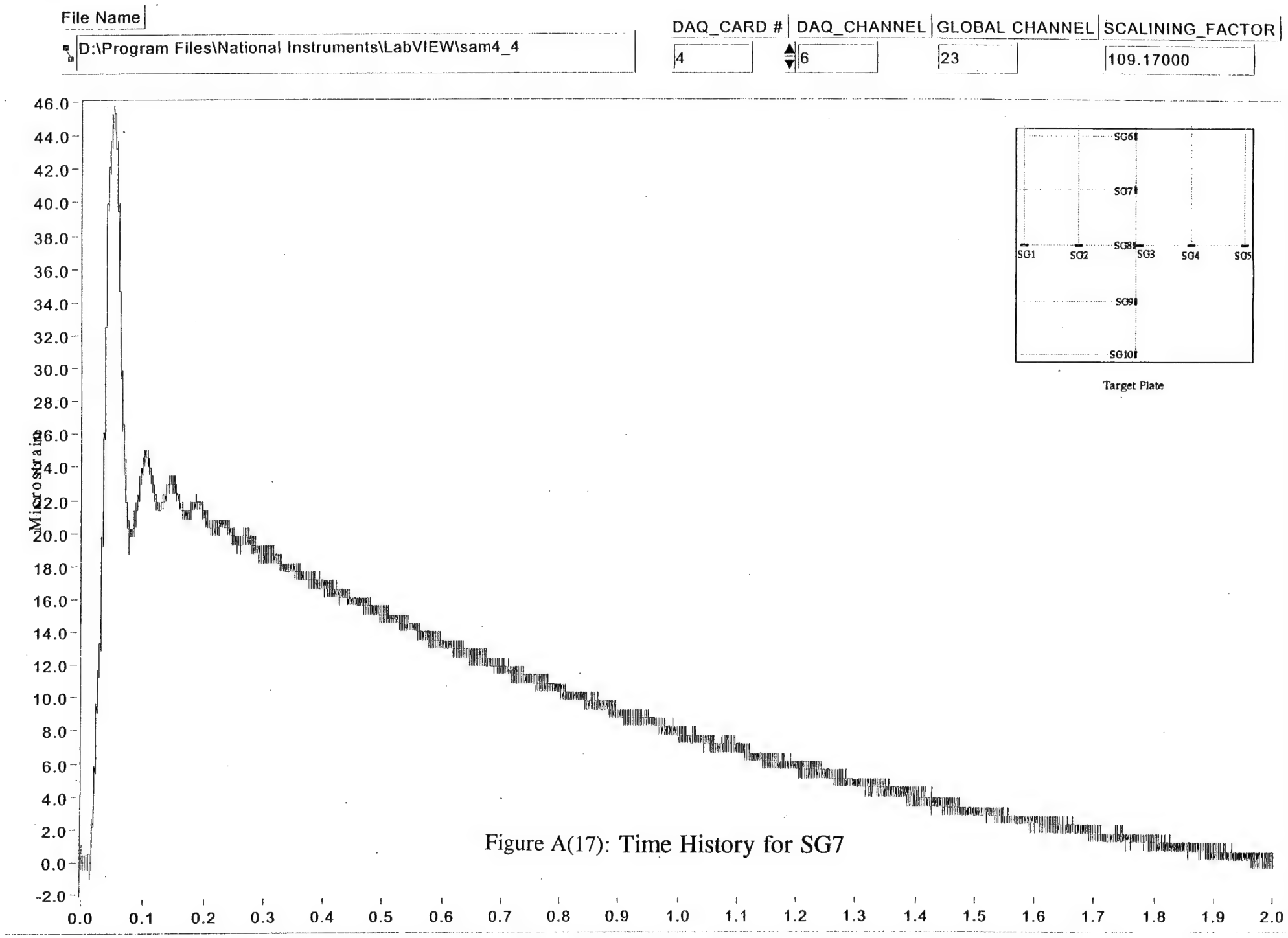

Figure A(17): Time History for SG7

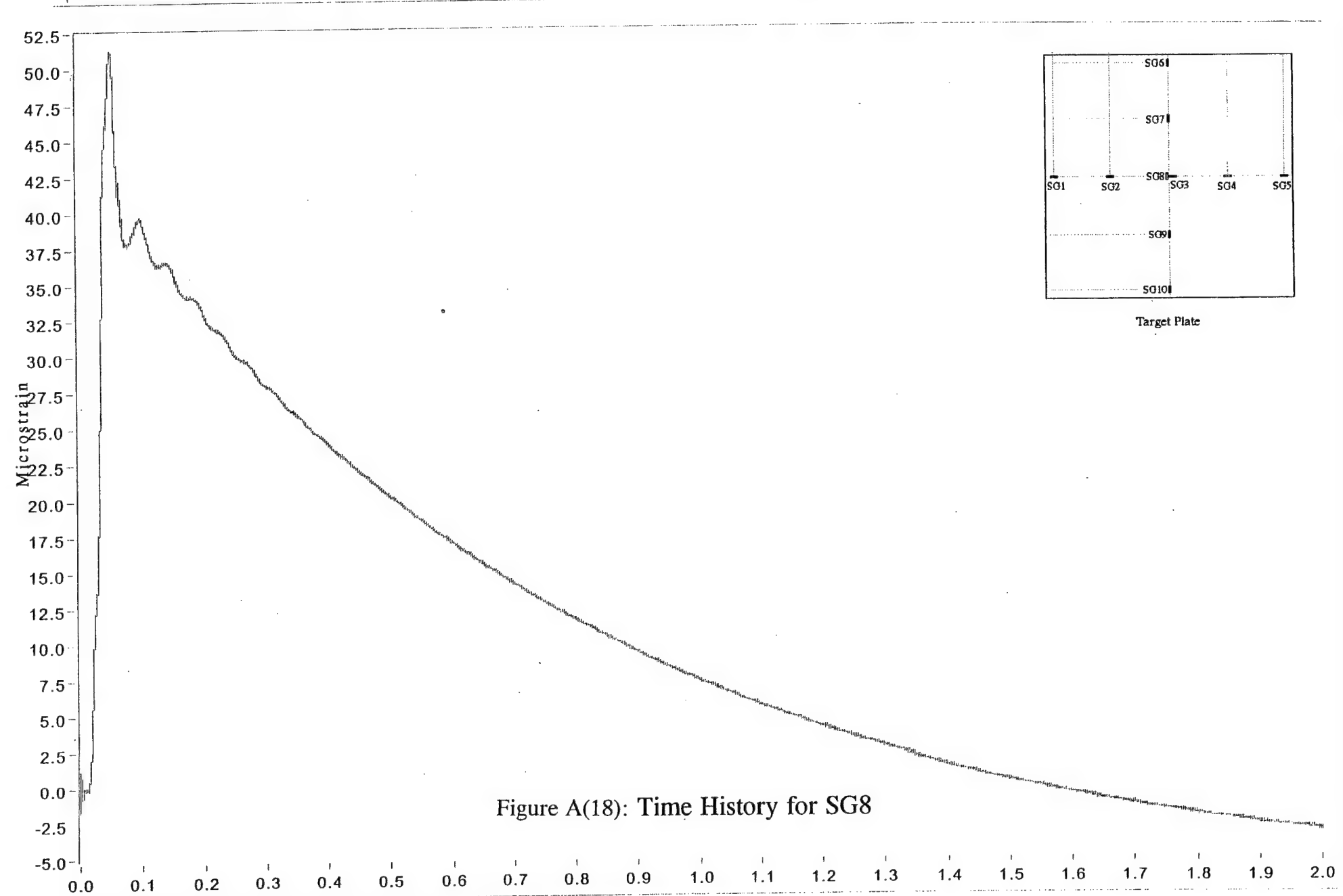

Figure A(18): Time History for SG8

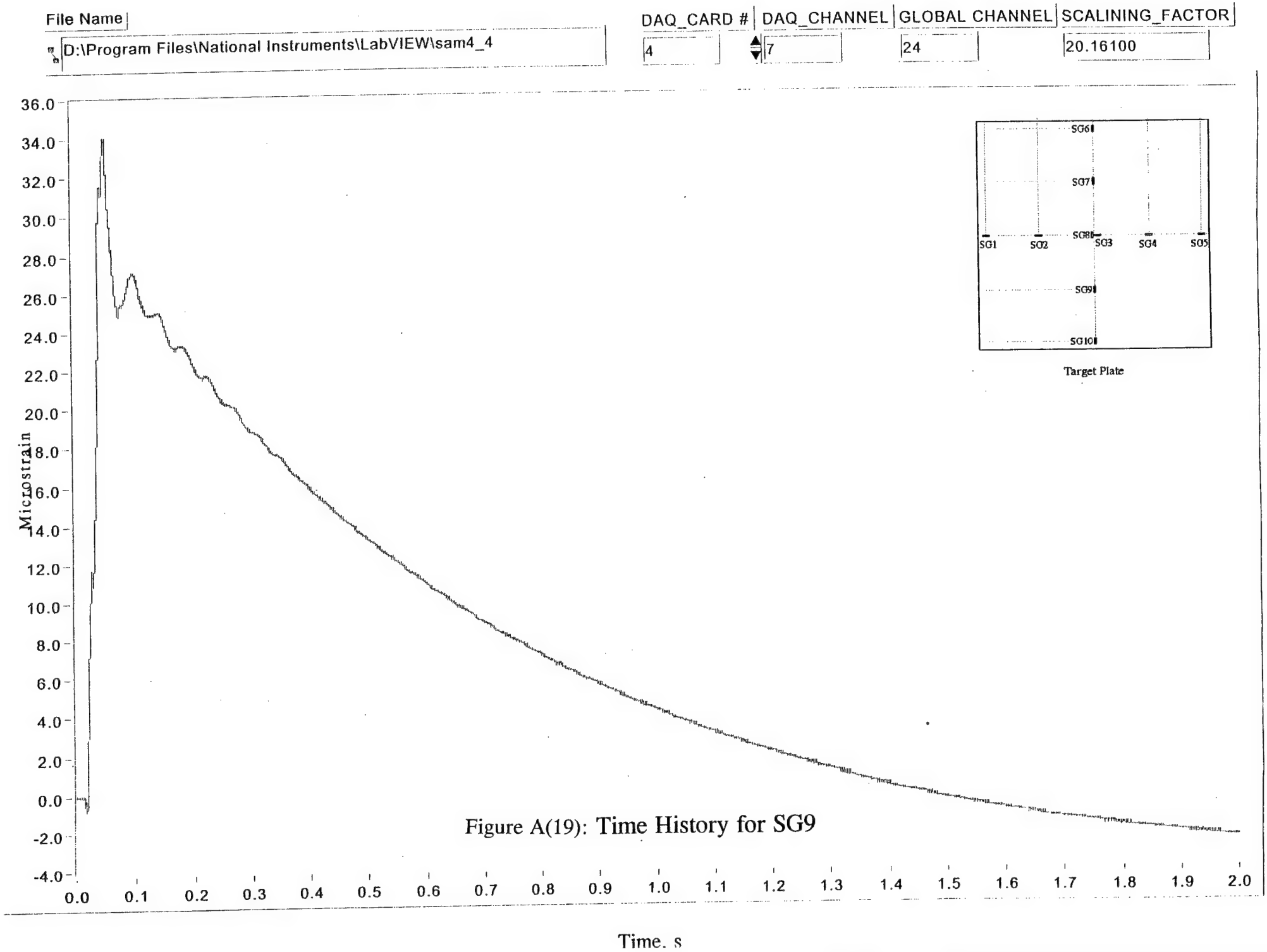

Figure A(19): Time History for SG9

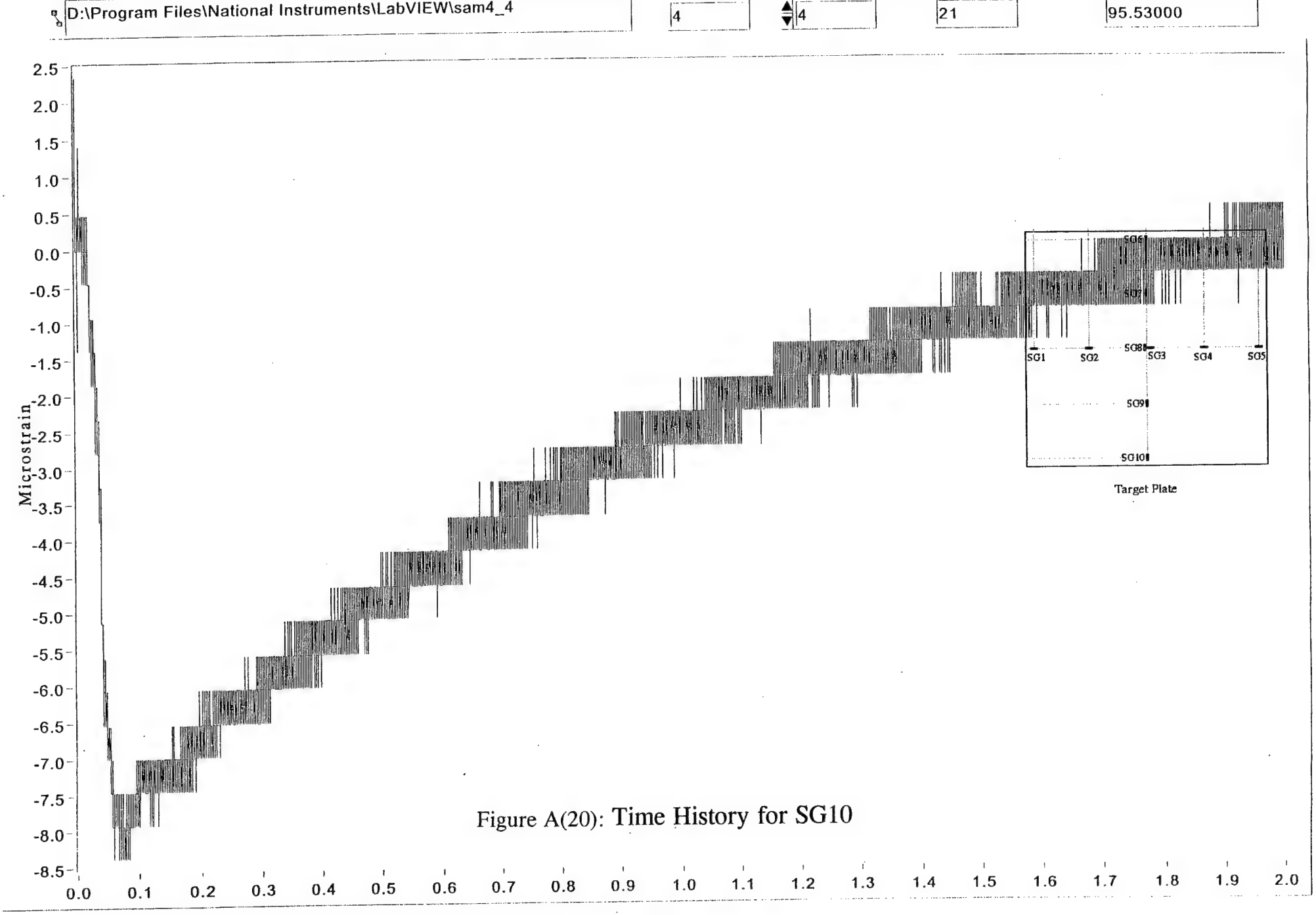

Figure A(20): Time History for SG10

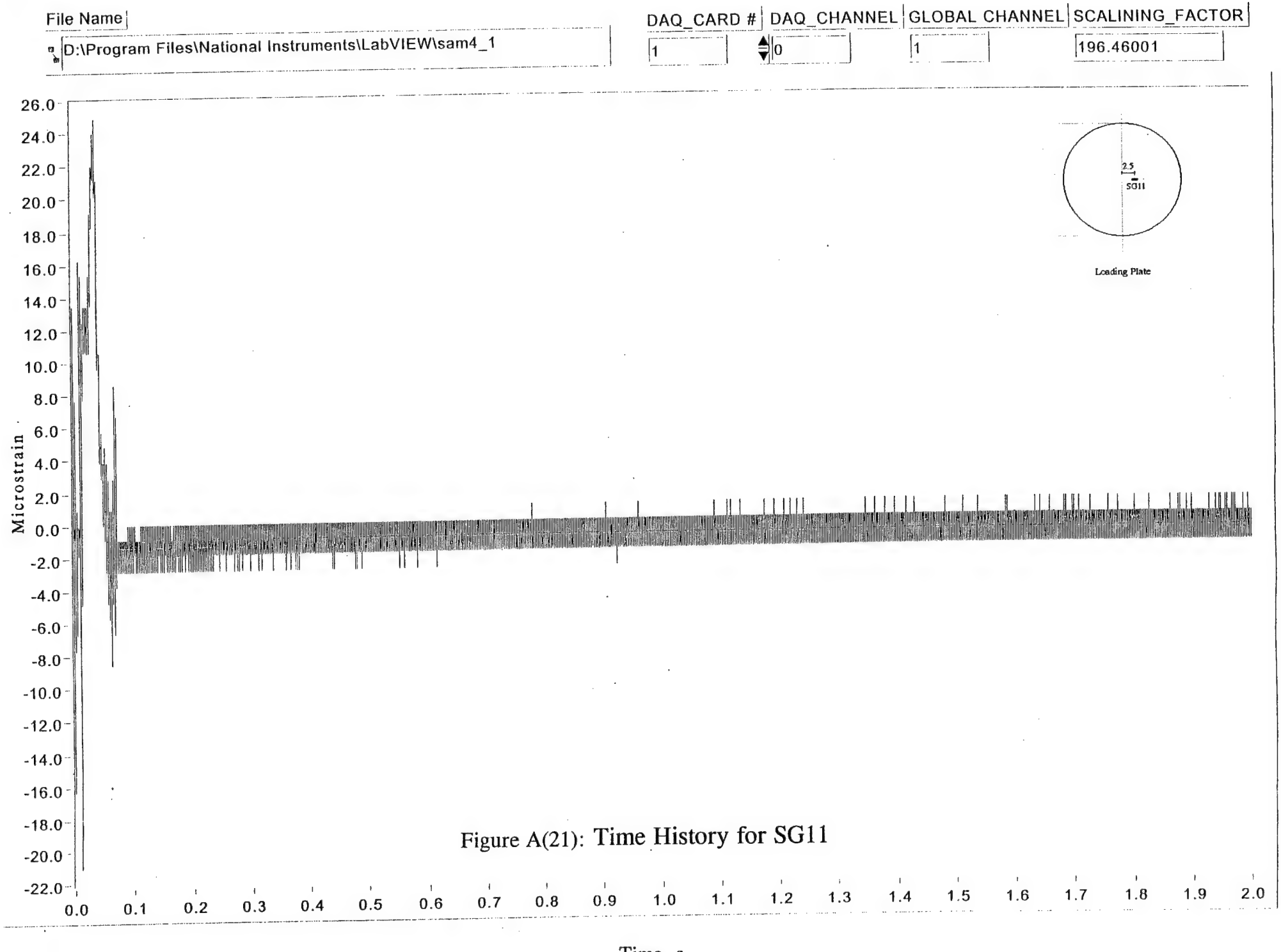

Figure A(21): Time History for SG11

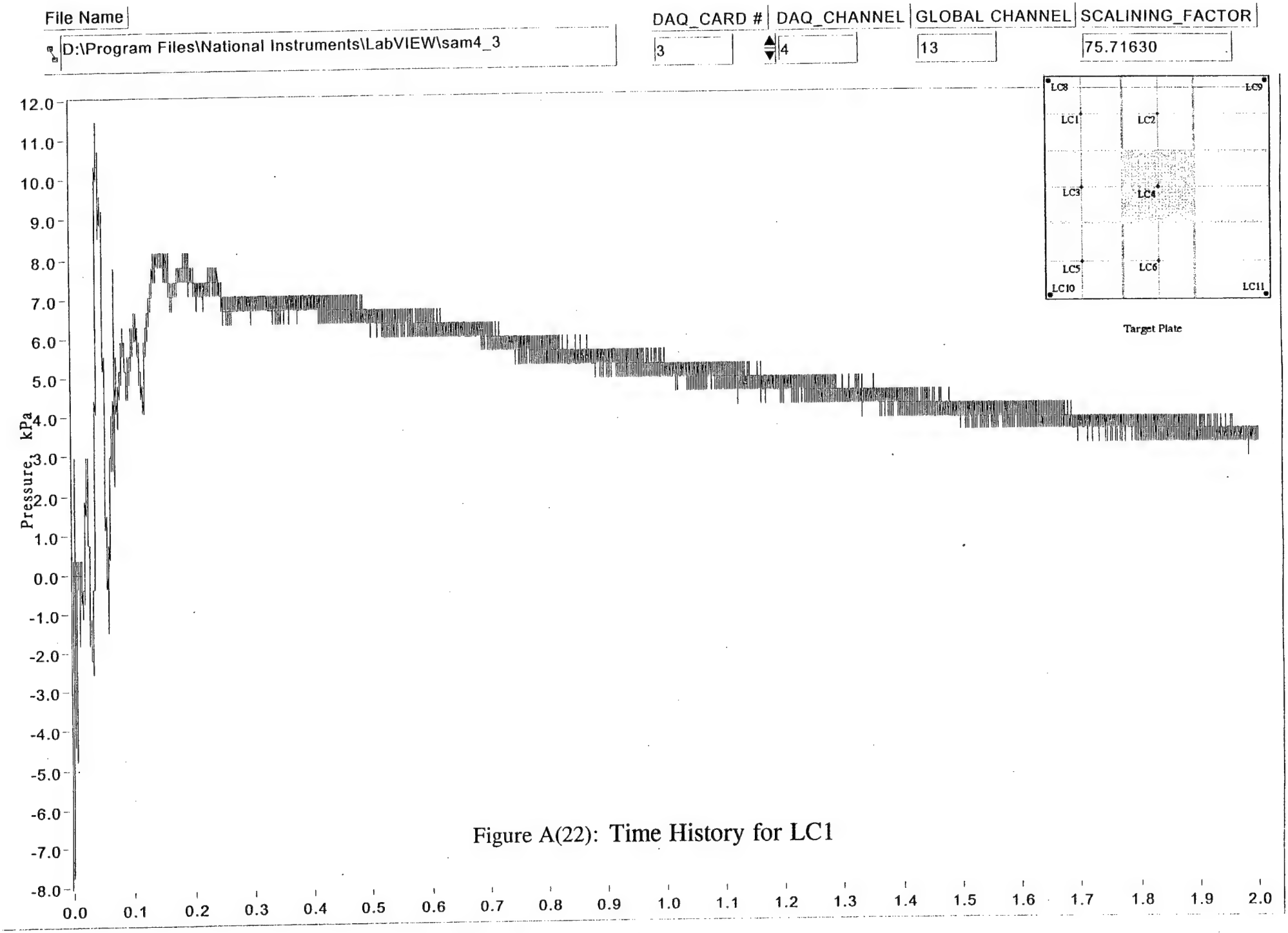

Figure A(22): Time History for LC1

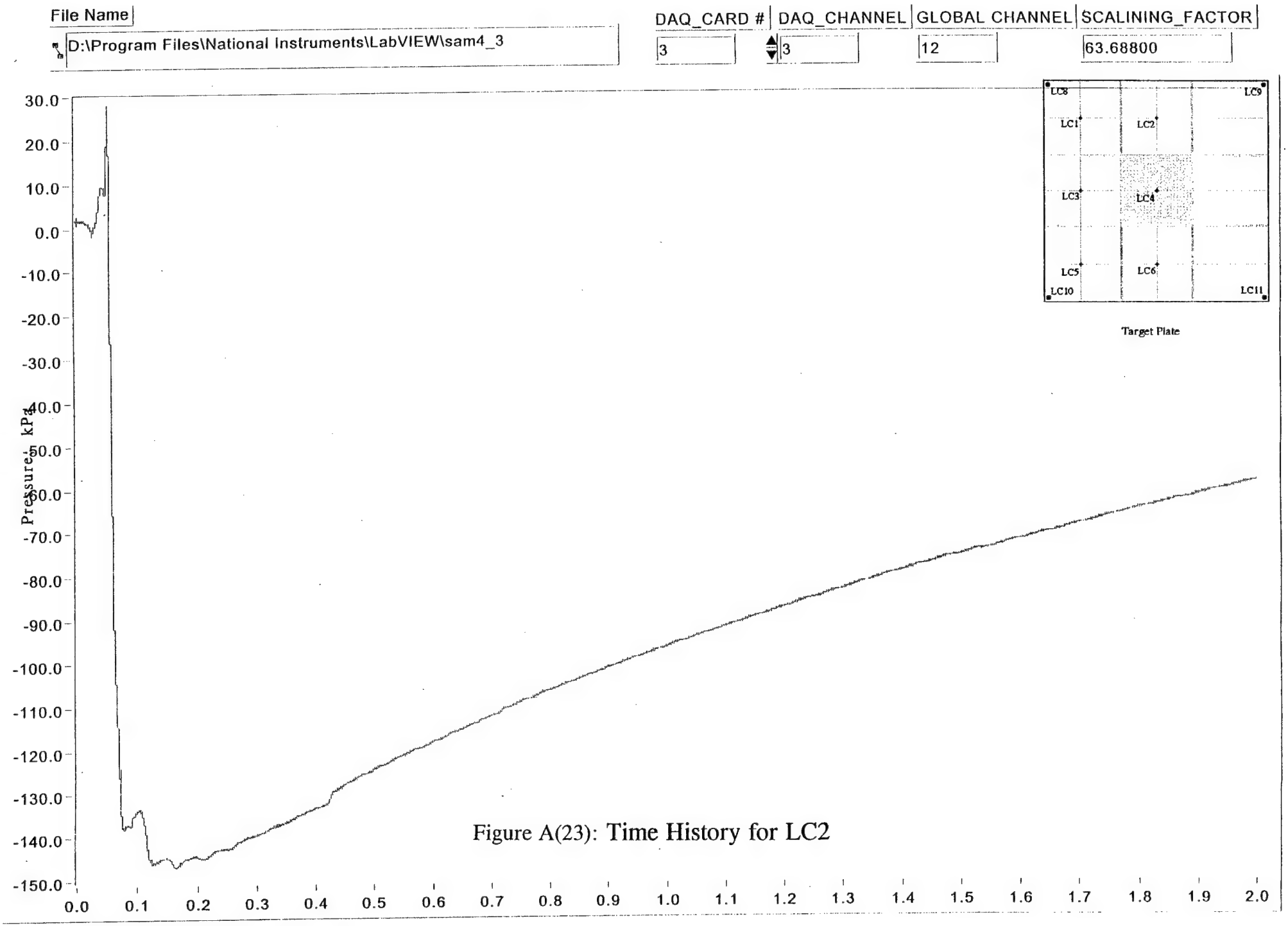

Figure A(23): Time History for LC2

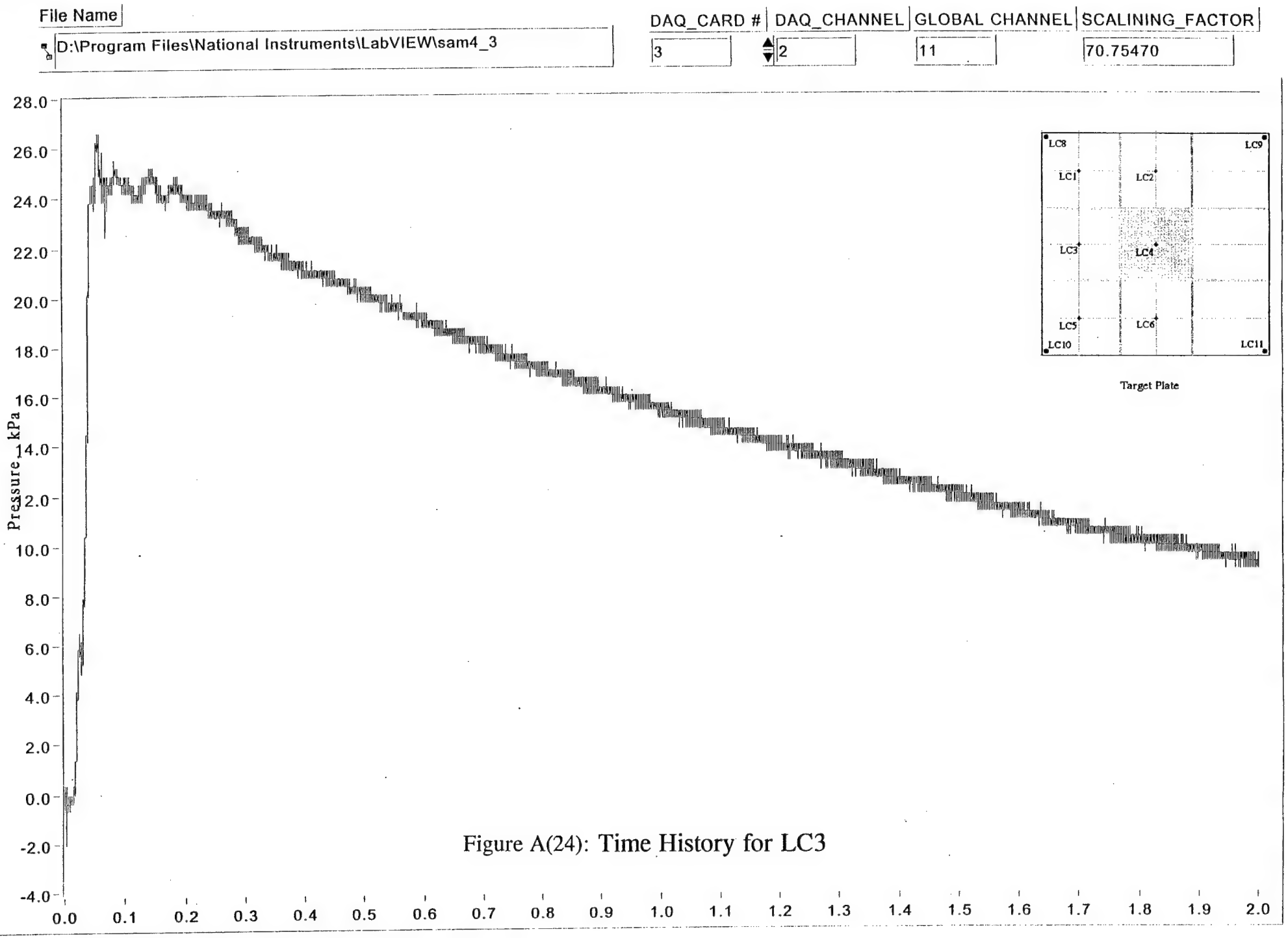

Figure A(24): Time History for LC3

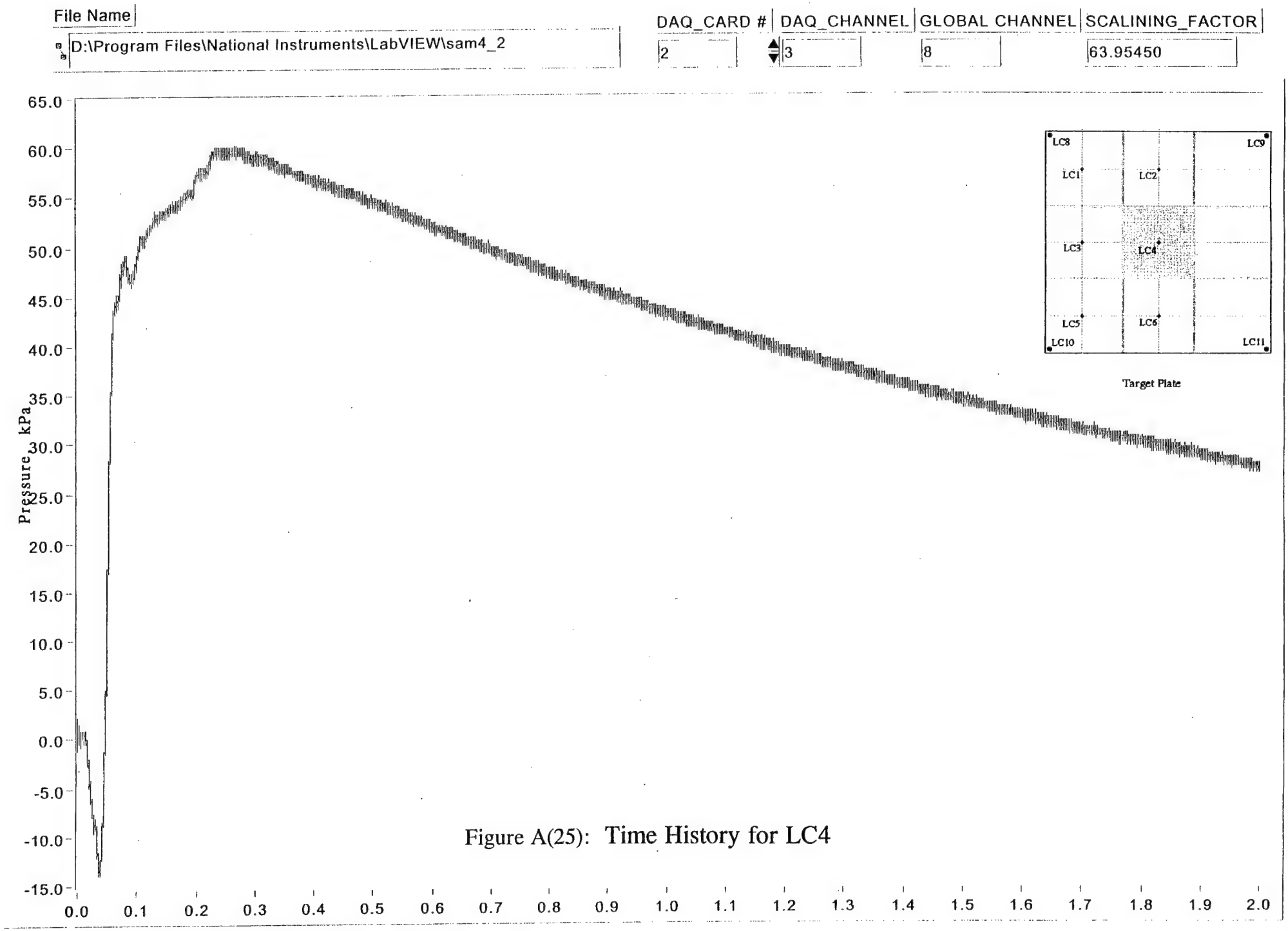

Figure A(25): Time History for LC4

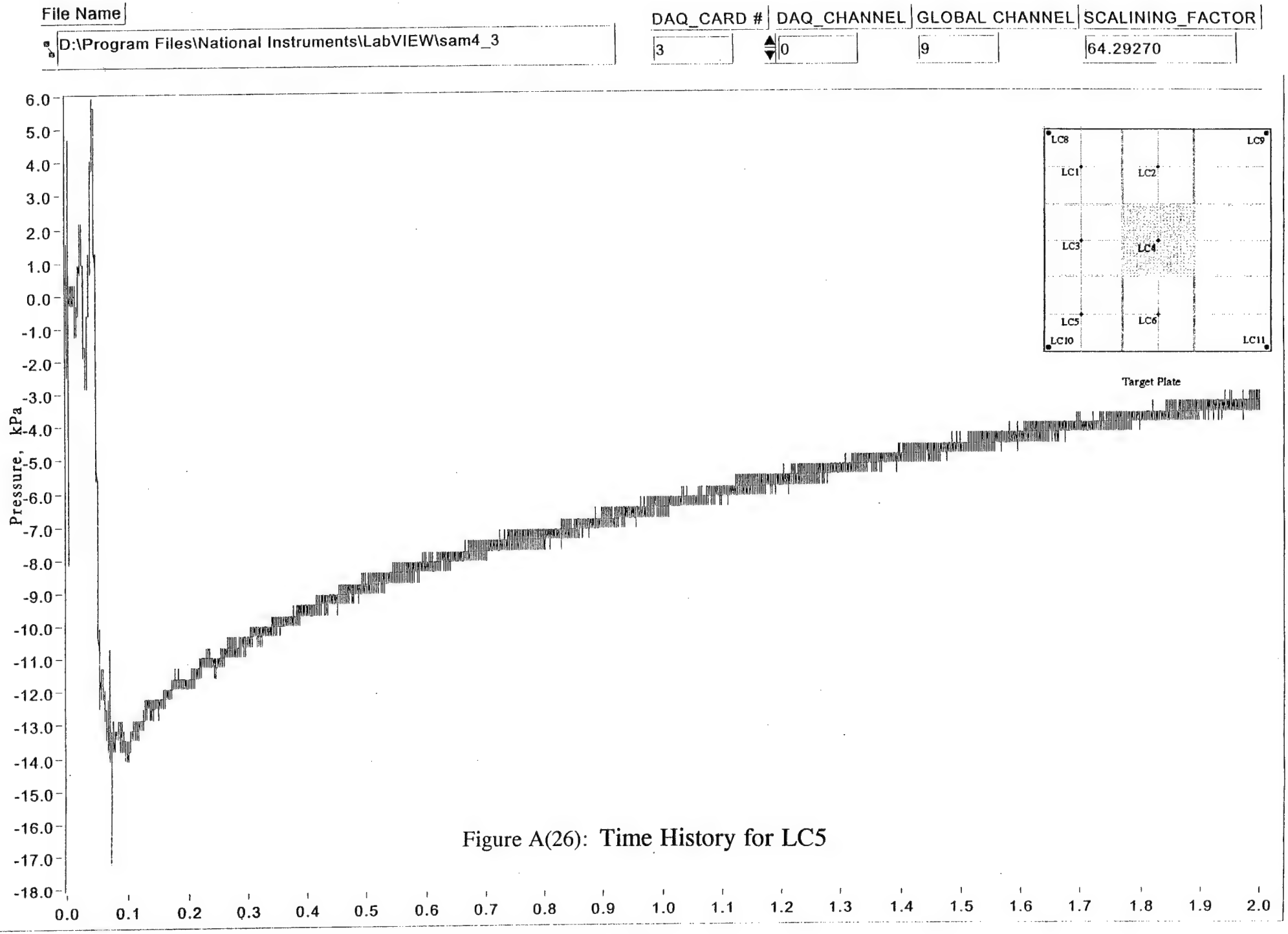

Figure A(26): Time History for LC5

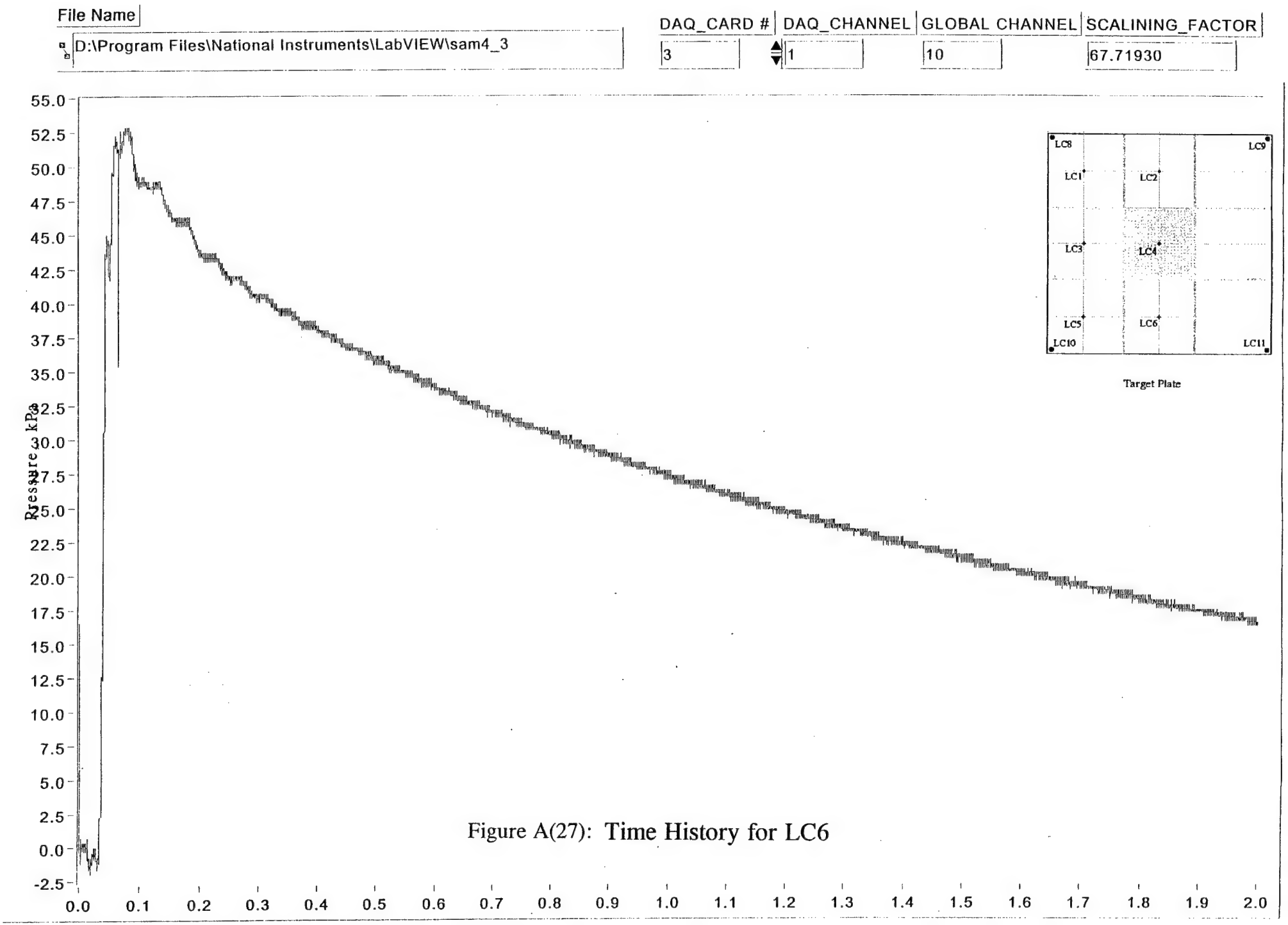

Figure A(27): Time History for LC6

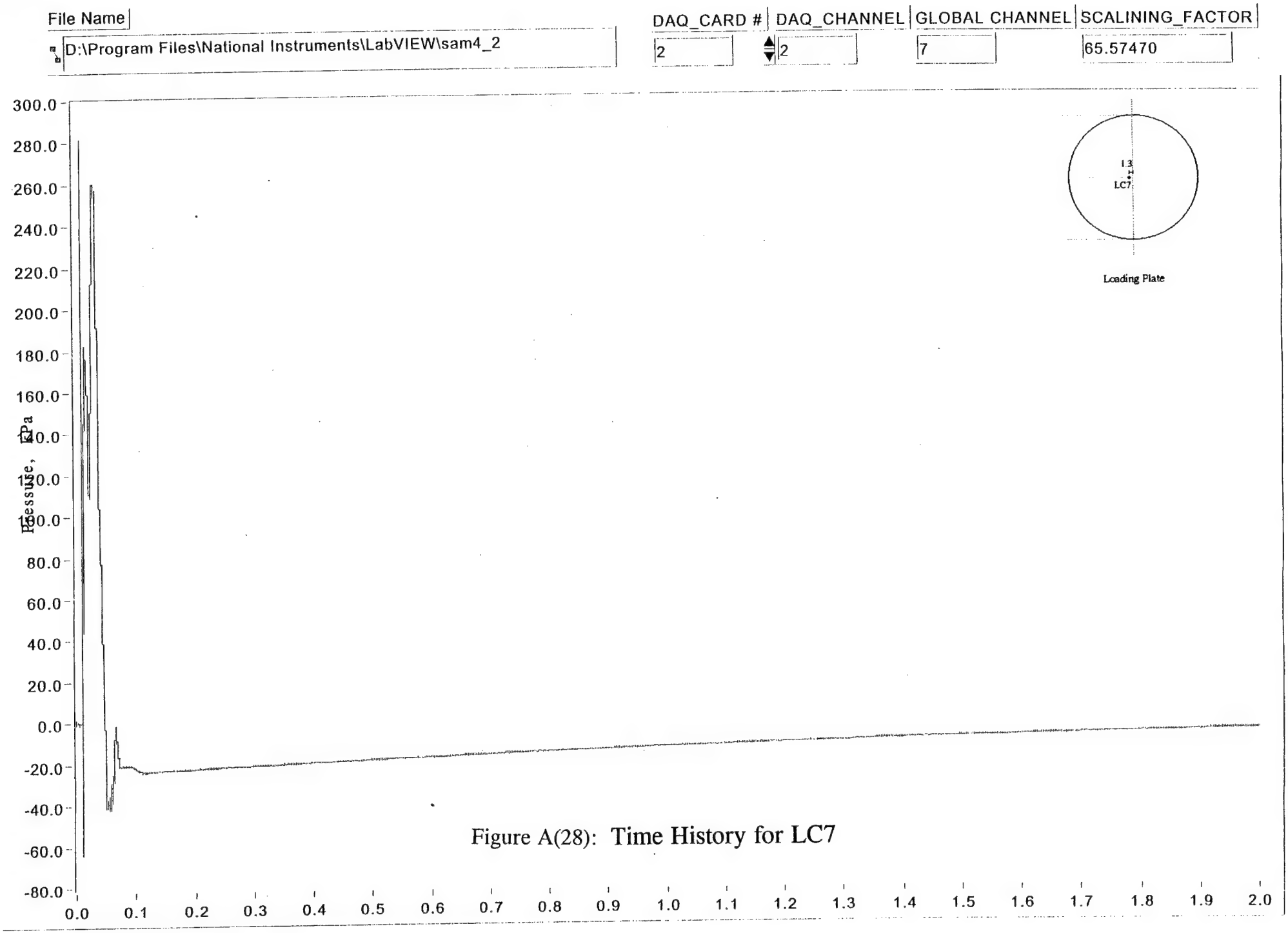

Figure A(28): Time History for LC7

File Name: D:\Program Files\National Instruments\LabVIEW\sam4_4

DAQ_CARD #	DAQ_CHANNEL	GLOBAL CHANNEL	SCALINING_FACTOR
4	0	17	10.74479

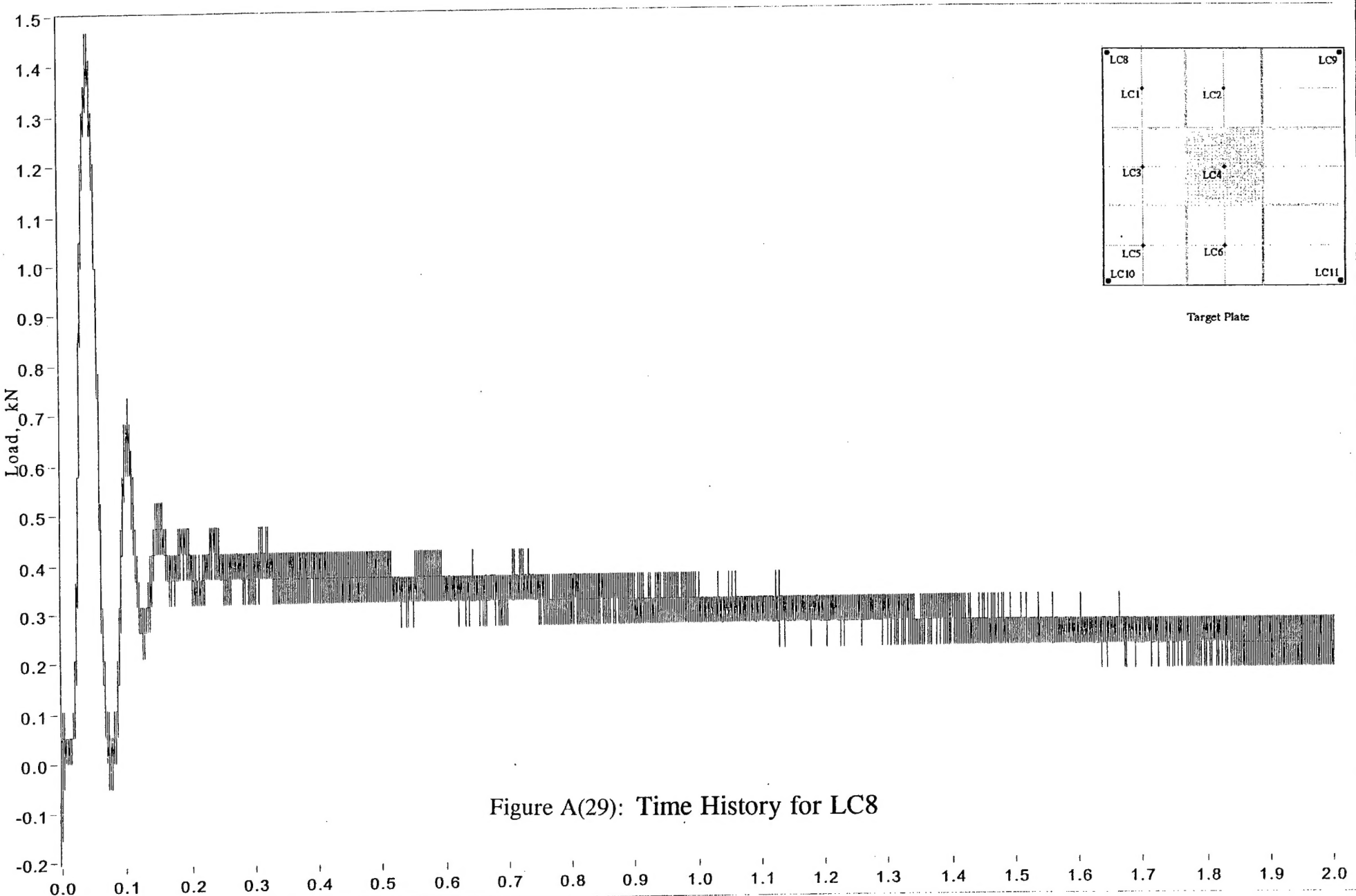

Figure A(29): Time History for LC8

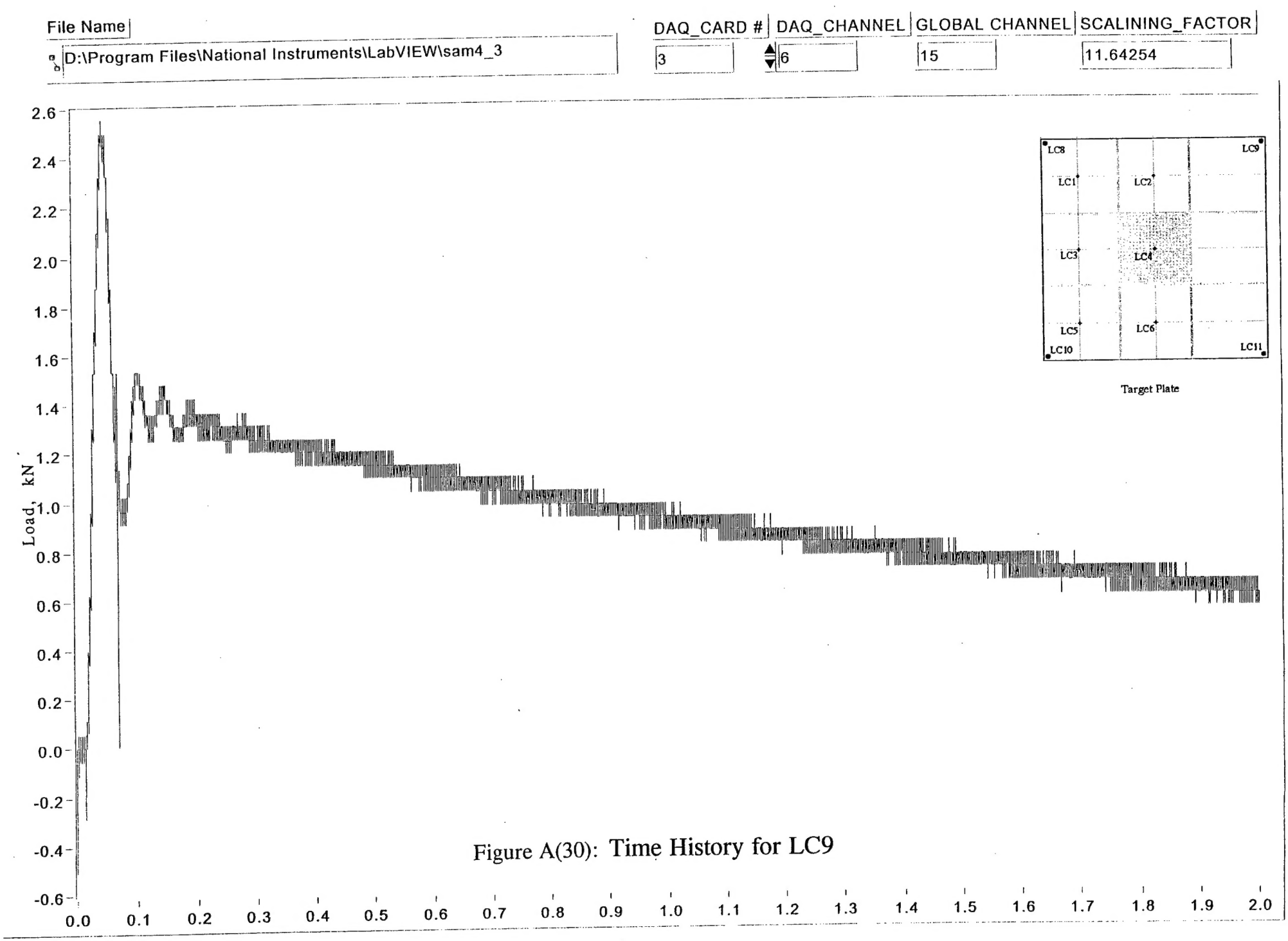

Figure A(30): Time History for LC9

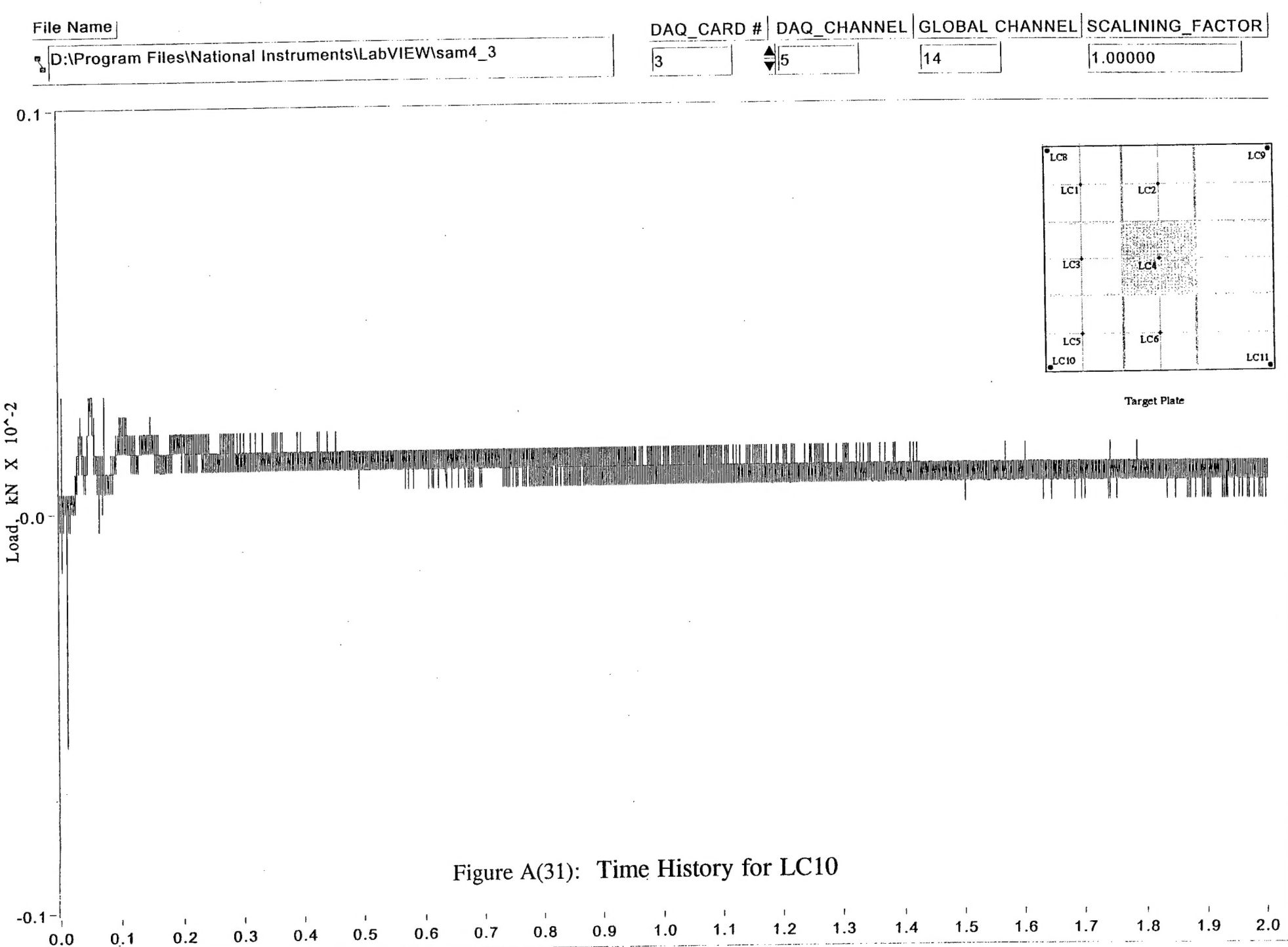

Figure A(31): Time History for LC10

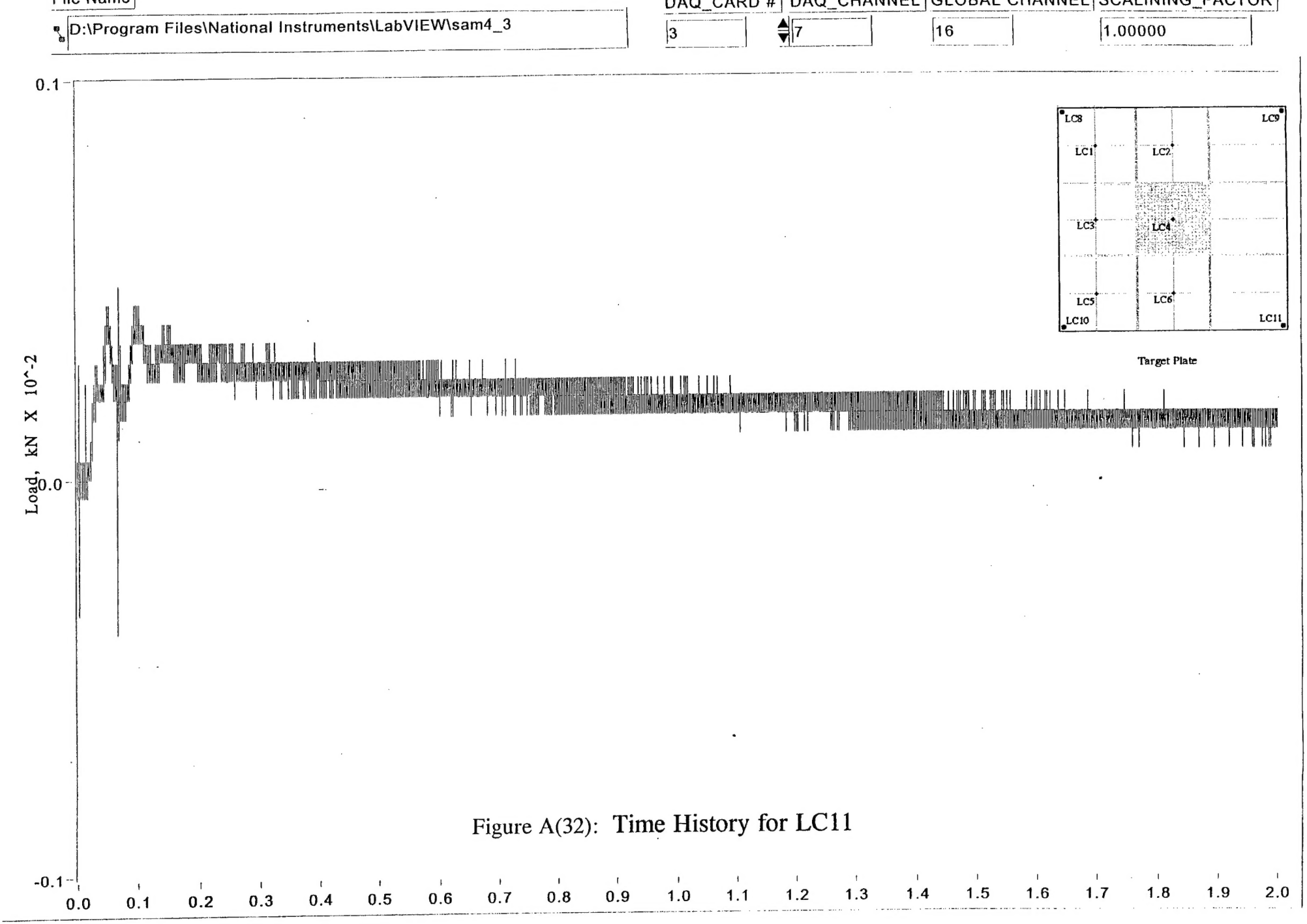

Figure A(32): Time History for LC11